

**Integrating Human and Machine Intelligence in Galaxy
Morphology Classification Tasks:
Development and Use Cases**

**A THESIS
SUBMITTED TO THE FACULTY OF THE GRADUATE SCHOOL
OF THE UNIVERSITY OF MINNESOTA
BY**

Melanie Renee Beck

**IN PARTIAL FULFILLMENT OF THE REQUIREMENTS
FOR THE DEGREE OF
Doctor of Philosophy**

**Advisor:
M. Claudia Scarlata**

August, 2017

© Melanie Renee Beck 2017
ALL RIGHTS RESERVED

Acknowledgements

Getting to this point in one's academic career requires the help and support of dozens of people. I hope I can name you all. Without a doubt in my mind, I know I would not be where I am today without my advisor, Claudia Scarlata. She unwittingly saved me from transferring to the Statistics department by asking me to join her research group and telling me that female astronomers need to stick together. She's right. I will forever be grateful to her because I know staying in this program was the right choice. In addition to the myriad technical skills I gained from her, above all Claudia taught me how to be an assertive, confident researcher – no bullshit. She pushed me when I needed pushing and stood back when I needed space. She taught me the value in finishing a project even if I didn't love it – publish! She also taught me how to navigate the sometimes turbulent interpersonal relationship between graduate student and advisor. I like to think we turned out not just as colleagues, but also friends (even if she does still get a little motherly..).

I must also thank my unofficial co-advisors, Lucy Fortson and Chris Lintott. Chris taught me how to work independently, how to speak up when I need help, how to effectively argue my position, and how to correctly interpret the British (do not underestimate how important this skill can be!). His ability to fit the pieces into the Big Picture helped me stay grounded. Lucy provided constant support. Her ability to navigate and communicate sdfasdfs

For the past three years I've had the delightful fortune to be part of the Galaxy Zoo science team. The galaxy zoo team including Brooke, Karen, Stephen, Becky The grad students: Micaela, Michael, Melanie, Tony, Brian

All the institutions that have contributed to funding me: Doctoral Dissertation Fellowship, Graduate School's Thesis Research Travel Grant, Oxford's Balzan Fellowship

My family for years and years of support.

Dedication

I dedicate this thesis to my brother, James Overton Beck IV, whose memory never ceases to inspire me to achieve.

Abstract

Quantifying galaxy morphology is a challenging yet scientifically rewarding task. As the scale of data continues to increase with upcoming surveys, traditional classification methods will struggle to handle the load. We present a solution through an integration of visual and automated classifications, preserving the best features of both human and machine. We demonstrate the effectiveness of such a system through a re-analysis of visual galaxy morphology classifications collected during the Galaxy Zoo 2 (GZ2) project. We reprocess the top-level question of the GZ2 decision tree with a Bayesian classification aggregation algorithm dubbed SWAP, originally developed for the Space Warps gravitational lens project. Through a simple binary classification scheme we increase the classification rate nearly 5-fold classifying 226,124 galaxies in 92 days of GZ2 project time while reproducing labels derived from GZ2 classification data with 95.7% accuracy.

We next combine this with a Random Forest machine learning algorithm that learns on a suite of non-parametric morphology indicators widely used for automated morphologies. We develop a decision engine that delegates tasks between human and machine and demonstrate that the combined system provides a factor of 11.4 increase in the classification rate, classifying 210,543 galaxies in just 32 days of GZ2 project time with 93.5% accuracy. As the Random Forest algorithm requires a minimal amount of computational cost, this result has important implications for galaxy morphology identification tasks in the era of *Euclid* and other large-scale surveys.

Contents

Acknowledgements	i
Dedication	iii
Abstract	iv
List of Tables	vii
List of Figures	viii
1 Introduction	1
1.1 Galaxy Zoo Express Overview	3
2 Bayesian aggregation of Galaxy Zoo classifications with SWAP	6
2.1 Galaxy Zoo 2 Classification Data	6
2.2 Efficiency through intelligent human-vote aggregation	7
2.2.1 Gold-standard sample	9
2.2.2 Fiducial SWAP simulation	10
2.2.3 Reducing human effort	14
2.2.4 Disagreements between SWAP and GZ2	16
2.2.5 Summary	17
2.3 Stuff from the appendix – fold into the main text	18
3 Measuring Nonparametric Morphological Diagnostics on SDSS Stamps	24
3.1 Introduction	24
3.2 Data	25

3.3	Image Cleaning	25
3.4	Morphology Diagnostics	25
3.5	Comparison with other samples	26
4	Combining nonparametric morphologies with human and machine intelligence	27
4.1	Efficiency through incorporation of machine classifiers	27
4.1.1	Random Forests	27
4.1.2	Grid Search and Cross-validation	28
4.1.3	Feature Representation and Pre-Processing	28
4.1.4	Decision Engine	30
4.1.5	The Machine Shop	31
4.2	Results	32
4.2.1	Who retires what, when?	33
4.2.2	Machine performance	34
4.3	Looking Forward	36
4.3.1	Conclusions	37
4.4	Acknowledgements	38
4.5	Stuff to fold into the existing text	39
5	A population of “clumpy” galaxies in local Universe	44
5.1	Sample Selection & Data	44
5.2	Analysis	46
5.2.1	Measuring clump radial distance	46
5.2.2	Clump H α H β ratios [Dust]	46
5.2.3	Clumpy H α equivalent widths	46
5.3	Discussion / Conclusions	46
6	Summary & Future Work	47
Appendix A. Spectro-polarimetry Confirms Central Powering in a Lyα Nebula at $z = 3.09$		54

List of Tables

4.1	Simulation summary	34
-----	------------------------------	----

List of Figures

1.1	Schematic of the human+machine hybrid system.	4
2.1	Galaxy Zoo volunteer confusion matrices achieved through SWAP. . . .	10
2.2	Galaxy posterior probabilities achieved through SWAP.	11
2.3	SWAP performance on Galaxy Zoo visual classifications.	12
2.4	SWAP volunteer weighting mechanism reduces human effort for classification	15
2.5	$f_{featured}$ distribution of SWAP misclassifications	16
2.6	SWAP performance does not dramatically change even with a range of input parameters (shaded regions) as compared to the fiducial run of Section 2.2.2 (dashed lines). <i>Left</i> . The quality (top) and retirement rate (bottom) when the confusion matrix is initialized as (0.4, 0.4) and (0.6, 0.6), with all other input parameters remaining constant. <i>Right</i> . Same as the left panel but allowing the subject prior probability, $p_0=0.2, 0.35$ and 0.8. Changing the confusion matrix has little impact on the quality of the labels but varies the total number of subjects retired. In contrast, changing the subject prior is more likely to affect the classification quality rather than the total number of subjects retired.	22

2.7	<i>Left.</i> Identifying ‘Featured’ subjects is independent of identifying ‘Not’ subjects. Both ROC curves use all subjects processed by SWAP where the score used to create the ROC curve is simply each subject’s achieved posterior probability. The Featured curve demonstrates how well we identify ‘Featured’ subjects with a threshold of 0.99, while the Not Featured curve demonstrates how well we identify ‘Not’ subjects with a threshold of 0.004. Typically, best performance is achieved by the score associated with the upper-left-most part of the curve. Our ‘Featured’ threshold is nearly optimal, while our ‘Not’ threshold could be improved since the blue square is not as close to the upper left hand corner as other possible values of the subject posterior. <i>Right.</i> Relation between measured morphology diagnostics for more than 280K SDSS galaxies. Most of these galaxies are processed through SWAP, receiving a posterior probability that estimates how likely each is to be ‘Featured’ or ‘Not’.	23
4.1	Random Forest learning curve	29
4.2	Performance of the human+machine combination – Galaxy Zoo: Express	30
4.3	Individual contributions of human and machine to galaxy classification	40
4.4	Random subsample of galaxy jpegs identified as false positives by the Random Forest	41
4.5	Distributions of measured galaxy morphology features	42
4.6	Random Forest’s feature importances	42

4.7 *Left.* Identifying ‘Featured’ subjects is independent of identifying ‘Not’ subjects. Both ROC curves use all subjects processed by SWAP where the score used to create the ROC curve is simply each subject’s achieved posterior probability. The Featured curve demonstrates how well we identify ‘Featured’ subjects with a threshold of 0.99, while the Not Featured curve demonstrates how well we identify ‘Not’ subjects with a threshold of 0.004. Typically, best performance is achieved by the score associated with the upper-left-most part of the curve. Our ‘Featured’ threshold is nearly optimal, while our ‘Not’ threshold could be improved since the blue square is not as close to the upper left hand corner as other possible values of the subject posterior. *Right.* Relation between measured morphology diagnostics for more than 280K SDSS galaxies. Most of these galaxies are processed through SWAP, receiving a posterior probability that estimates how likely each is to be ‘Featured’ or ‘Not’. 43

Chapter 1

Introduction

Here we define the big overarching problem.

Why classify galaxies?

What classifications are needed?

How do we get these classifications?

What problems do traditional methods face?

Chapter on a literature study of machine learning in astronomy? Or just in galaxy classification? And some machine learning basics.

Chapter that is essentially my paper but with an added section on the exploration of dimensionality reduction algorithms we explored.

Chapter on the science case of rare clumpy galaxies in the local universe found thanks to GZH.

Appendix: Stupid spectro-polarimetry paper

We're going to add in all the shit that I've done in the past three years – much of that didn't make it into my paper. We can break up the work into two major parts:

1. SWAP + GZ

BEEF THIS UP.

Astronomers have made use of visual galaxy morphologies to understand the dynamical structure of these systems for nearly ninety years (e.g., Hubble, 1936; de Vaucouleurs, 1959; Sandage, 1961; van den Bergh, 1976; Nair & Abraham, 2010; Baillard et al., 2011).

The division between early-type and late-type systems corresponds, for example, to a wide range of parameters from mass and luminosity, to environment, colour, and star formation history (e.g., Kormendy, 1977; Dressler, 1980; Strateva et al., 2001; Blanton et al., 2003; Kauffmann et al., 2003; Nakamura et al., 2003; Shen et al., 2003; Peng et al., 2010); while detailed observations of morphological features such as bars and bulges provide information about the history of their host systems (e.g., review by Kormendy & Kennicutt, 2004; Elmegreen et al., 2008; Sheth et al., 2008; Masters et al., 2011; Simmons et al., 2014). Modern studies of morphology divide systems into broad classes (e.g., Conselice, 2006; Lintott et al., 2008; Kartaltepe et al., 2015; Peth et al., 2016), but a wealth of information can be gained from identifying new and often rare classes, such as low redshift clumpy galaxies (e.g., Elmegreen et al., 2013), polar-ring galaxies (e.g., Whitmore et al., 1990), and the green peas (Cardamone et al., 2009).

While the Galaxy Zoo project has provided a solution that scales visual classification for current surveys by harnessing the combined power of thousands of volunteers (Lintott et al., 2008, 2011; Willett et al., 2013, 2017; Simmons et al., 2017), producing a prolific amount of scientific output (e.g., Land et al., 2008; Bamford et al., 2009; Darg et al., 2010; Schawinski et al., 2014; Galloway et al., 2015; Smethurst et al., 2016); upcoming surveys such as *LSST* and *Euclid* will require a different approach, imaging more than a billion new galaxies (LSST Science Collaboration et al., 2009; Laureijs et al., 2011). If detailed morphologies can be extracted for just 0.1% of this imaging, we will have millions of images to contend with. A project of this magnitude would take more than sixty years to classify at Galaxy Zoo’s current rate and configuration. Standard visual morphology methods will thus be unable to cope with the scale of data.

Another approach has been the automated extraction of morphologies with the development of parametric (Sersic, 1968; Odewahn et al., 2002; Peng et al., 2002), and non-parametric (Abraham et al., 1994; Conselice, 2003; Abraham et al., 2003; Lotz et al., 2004; Freeman et al., 2013) structural indicators. While these scale well to large samples (e.g., Simard et al., 2011; Griffith et al., 2012; Casteels et al., 2014; Holwerda et al., 2014; Meert et al., 2016), they often fail to capture detailed structure and can provide only statistical morphologies with large uncertainties (e.g., Abraham et al., 1996; Bershadsky et al., 2000).

Machine learning techniques are becoming increasingly popular for classification and

image processing tasks. Another automated approach, these generally work by defining a set of features that describe the morphology in an N -dimensional space. The location in this morphology space defines a morphological type for each galaxy. Learning the morphology space can be achieved through algorithms such as Support Vector Machines (Huertas-Company et al., 2008) or Principal Component Analysis (Watanabe et al., 1985; Scarlata et al., 2007). Another approach is through deep learning, a machine learning technique that attempts to model high level abstractions. Algorithms like convolutional and artificial neural networks (CNNs, ANNs) have been used for galaxy morphology classification with impressive accuracy (Ball et al., 2004; Banerji et al., 2010; Dieleman et al., 2015; Huertas-Company et al., 2015). A drawback to all machine learning classification techniques is the need for standardized training data, with more complex algorithms requiring more data. Furthermore, these data must be consistent for each survey: differences in resolution and depth can be implicitly learned by the algorithm making their application to disparate surveys challenging.

In this work we present a system that preserves the best features of both visual and automatic classifications, developing for the first time a framework that brings both human and machine intelligence to the task of galaxy morphology to handle the scale and scope of next generation data. We demonstrate the effectiveness of such a system through a re-analysis of visual galaxy morphology classifications collected during the Galaxy Zoo 2 project, and combine these with a Random Forest machine learning algorithm that trains on a suite of non-parametric morphology indicators widely used for automated morphologies. In this paper we focus on the first question of the Galaxy Zoo decision tree. We demonstrate that our method provides a factor of 11.4 increase in the rate of galaxy morphology classification while maintaining at least 93.5% classification accuracy as compared to Galaxy Zoo 2 published data. We first present an overview of our framework, which also serves as a blueprint for this paper.

1.1 Galaxy Zoo Express Overview

The Galaxy Zoo Express (GZX) framework combines human and machine to increase morphological classification efficiency, both in terms of the classification rate and required human effort. Figure 1.1 presents a schematic of GZX including section numbers

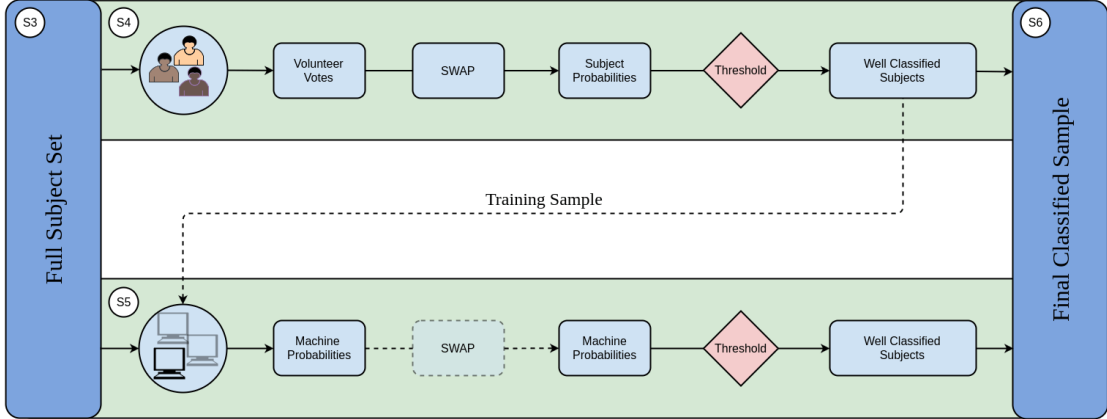


Figure 1.1 Schematic of our hybrid system. Humans provide classifications of galaxy images via a web interface. We simulate this with the Galaxy Zoo 2 classification data described in Section 2.1. Human classifications are processed with an algorithm described in Section 2.2. Subjects that pass a set of thresholds are considered human-retired (fully classified) and provide the training sample for the machine classifier as described in Section 4.1. The trained machine is applied to all subjects not yet retired. Those that pass an analogous set of machine-specific thresholds are considered machine-retired. The rest remain in the system to be classified by either human or machine. This procedure is repeated nightly. Our results are reported in Section 4.2.

as a shortcut for the reader. We note that transparent portions of the schematic represent areas of future work which we explore in Section 4.3. Any system combining human and machine classifications will have a set of generic features: a group of human classifiers, at least one machine classifier, and a decision engine which determines how these classifications should be combined.

In this work we demonstrate our system through a re-analysis of Galaxy Zoo 2 (GZ2) classifications. This allows us to create simulations of human classifiers (described in Section 2.1). These classifications are used most effectively when processed with SWAP, a Bayesian code described in Section 2.2, first developed for the Space Warps gravitational lens discovery project (Marshall et al., 2016). These subjects provide the machine’s training sample.

In Section 4.1, we incorporate a machine classifier. We have developed a Random Forest algorithm that trains on measured morphology indicators such as Concentration,

Asymmetry, Gini coefficient and M_{20} well-suited for the top-level question of the GZ2 decision tree, discussed below. After a sufficient number of subjects have been classified by humans, the machine is trained and its performance assessed through cross-validation. This procedure is repeated nightly and the machine’s performance increases with size of the training sample, albeit with a performance limit. Once the machine reaches an acceptable level of performance it is applied to the remaining galaxy sample.

Even with this simple description, one can see that the classification process will progress in three phases. First, the machine will not yet have reached an acceptable level of performance; only humans contribute to subject classification. Second, the machine’s performance will improve; both humans and machine will be responsible for classification. Finally, machine performance will slow; remaining images will likely need to be classified by humans. These results are explored in Section 4.2. This blueprint allows even modest machine learning routines to make significant contributions alongside human classifiers and removes the need for ever-increasing performance in machine classification.

Chapter 2

Bayesian aggregation of Galaxy Zoo classifications with SWAP

2.1 Galaxy Zoo 2 Classification Data

Our simulations utilize original classifications made by volunteers during the GZ2 project. These data¹ are described in detail in Willett et al. (2013), though we provide a brief overview here. The GZ2 subject sample consists of 285,962 galaxies identified as the brightest 25% (r -band magnitude < 17) residing in the SDSS North Galactic Cap region from Data Release 7 and included subjects with both spectroscopic and photometric redshifts out to $z < 0.25$. Subjects were shown as colour composite images via a web-based interface² wherein volunteers answered a series of questions pertaining to the morphology of the subject. With the exception of the first question, subsequent queries were dependent on volunteer responses from the previous task creating a complex decision tree³. Using GZ2 nomenclature, a *classification* is the total amount of information about a subject obtained by completing all tasks in the decision tree. A subject is *retired* after it has achieved a sufficient number of classifications.

For our current analysis, we choose the first task in the tree: “Is the galaxy simply smooth and rounded, with no sign of a disk?” to which possible responses include

¹ data.galaxyzoo.org

² www.galaxyzoo.org

³ A visualization of this decision tree can be found at https://data.galaxyzoo.org/gz_trees/gz_trees.html

“smooth”, “features or disk”, or “star or artifact”. This choice serves two purposes: 1) this is one of only two questions in the GZ2 decision tree that is asked of every subject thus maximizing the amount of data we have to work with, and 2) our analysis assumes a binary task and this question is simple enough to cast as such. Specifically, we combine “star or artifact” responses with “features or disk” responses.

We assign each subject a descriptive label in order to compare our classification output with GZ2. GZ2 classifications are composed of volunteer vote fractions for each response to every task in the decision tree, denoted as f_{response} . They are derived from the fraction of volunteers who voted for a particular response and are thus approximately continuous. A common technique is to place a threshold on these vote fractions to select samples with an emphasis on purity or completeness, depending on the science case. For our current analysis we choose a threshold of 0.5, that is, if $f_{\text{featured}} + f_{\text{artifact}} > f_{\text{smooth}}$, the galaxy is labelled ‘Featured’, otherwise it is labelled ‘Not’. Though naive, we will demonstrate that this threshold produces adequate results, though a more sophisticated mechanism will be explored in a future publication. We note that only 512 subjects in the GZ2 catalogue have a majority f_{artifact} , contributing less than half a percent contamination by combining the “star or artifact” with “features or disk” responses.

The GZ2 catalogue publishes three types of vote fractions for each subject: raw, weighted, and debiased. Debiased vote fractions are calculated to correct for redshift bias, a task that GZX does not perform. The weighted vote fractions account for inconsistent volunteers. The SWAP algorithm (described below) also has a mechanism to weight volunteer votes, however, the two methods are in stark contrast. For consistency, we derive labels from the raw vote fractions (GZ2_{raw}) that have received no post-processing whatsoever. In total, the data consist of over 16 million classifications from 83,943 individual volunteers.

2.2 Efficiency through intelligent human-vote aggregation

Galaxy Zoo 2 had a brute-force subject retirement rule whereby each galaxy was to receive approximately forty independent classifications. Once the project reached completion, inconsistent volunteers were down-weighted (Willett et al., 2013), a process that does not make efficient use of those who are exceptionally skilled. To intelligently

manage subject retirement and increase classification efficiency, we adapt an algorithm from the Zooniverse project Space Warps (Marshall et al., 2016), which searched for and discovered several gravitational lens candidates in the CFHT Legacy Survey (More et al., 2016). Dubbed SWAP (Space Warps Analysis Pipeline), this algorithm computed the probability that an image contained a gravitational lens given volunteers’ classifications and experience after being shown a training sample consisting of simulated lensing events. We provide a brief overview here.

The algorithm assigns each volunteer an *agent* which interprets that volunteer’s classifications. Each agent assigns a 2×2 confusion matrix to their volunteer which encodes that volunteer’s probability of correctly identify feature A given that the subject exhibits feature A ; and the probability of correctly identifying the absence of feature A (denoted N) given that the subject does not exhibit that feature. The agent updates these probabilities by estimating them as

$$P(\text{“}X\text{”}|X, \mathbf{d}) \approx \frac{\mathcal{N}_{\text{“}X\text{”}}}{\mathcal{N}_X} \quad (2.1)$$

where X is the true classification of the subject and “ X ” is the classification made by the volunteer upon viewing the subject. Thus $\mathcal{N}_{\text{“}X\text{”}}$ is the number of classifications the volunteer labelled as type X , \mathcal{N}_X is the number of subjects the volunteer has seen that were actually of type X , and \mathbf{d} represents the history of the volunteer, i.e., all subjects they have seen. Therefore the confusion matrix for a single volunteer goes as

$$\mathcal{M} = \begin{bmatrix} P(\text{“}A\text{”}|N, \mathbf{d}) & P(\text{“}A\text{”}|A, \mathbf{d}) \\ P(\text{“}N\text{”}|N, \mathbf{d}) & P(\text{“}N\text{”}|A, \mathbf{d}) \end{bmatrix} \quad (2.2)$$

where probabilities are normalised such that $P(\text{“}A\text{”}|A) = 1 - P(\text{“}N\text{”}|A)$.

Each subject is assigned a prior probability that it exhibits feature A : $P(A) = p_0$. When a volunteer makes a classification, Bayes’ theorem is used to compute how that subject’s prior probability should be updated into a posterior using elements of the agent’s confusion matrix. As the project progresses, each subject’s posterior probability is updated after every volunteer classification, nudged higher or lower depending on volunteer input. Upper and lower probability thresholds can be set such that when a subject’s posterior crosses the upper threshold it is highly likely to exhibit feature A ; if

it crosses the lower threshold it is highly likely that feature A is absent. Subjects whose posteriors cross either of these thresholds are considered retired.

2.2.1 Gold-standard sample

BULK UP THIS SECTION – add sample selection figures, comparison with Nair catalog, potential volunteer biases...

A key feature of the original Space Warps project was the training of individual volunteers through the use of simulated images. These were interspersed with real imaging and were predominantly shown at the beginning of a volunteer’s association with the project, allowing that volunteer’s agent time to update before classifying real data. Volunteers were provided feedback in the form of a pop-up comment after classifying a training image. GZ2 did not train volunteers in such a way, presenting a challenge when applying SWAP to GZ2 classifications. Though we cannot retroactively train GZ2 volunteers, we develop a gold standard sample and arrange the order of gold standard classifications in order to mimic the Space Warps system.

We create a gold standard sample by selecting 3496 SDSS galaxies representative of the relative abundance of T-Types, a numerical index of a galaxy’s stage along the Hubble sequence, at $z \sim 0$ by considering galaxies that overlap with the Nair & Abraham (2010) catalogue, a collection of $\sim 14\text{K}$ galaxies classified by eye into T-Types. We generate expert labels for these galaxies that are consistent with the labels we defined for GZ2 classifications. These are obtained through the Zooniverse platform⁴ from 15 professional astronomers, including members of the Galaxy Zoo science team. The question posed was identical to the original top-level GZ2 question and at least five experts classified each galaxy. Votes are aggregated and a simple majority provides an expert label for each subject. This ensures that our expert labels are defined in exactly the same manner as the labels we assign the rest of the GZ2 sample. Our final dataset consists of the GZ2 classifications made by those volunteers who classify at least one of these gold standard subjects. We thus retain for our simulation 12,686,170 classifications from 30,894 unique volunteers. When running SWAP, classifications of gold standard subjects are always processed first.

⁴ The Project Builder template facility can be found at <http://www.zooniverse.org/lab>.

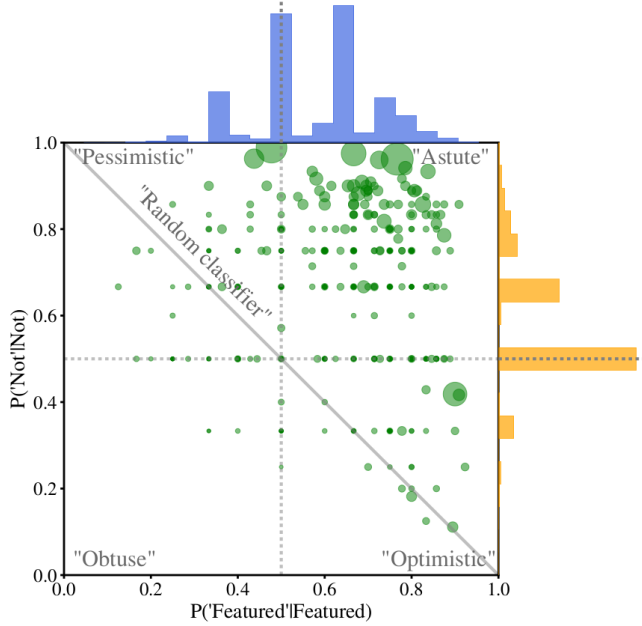


Figure 2.1 Confusion matrices for 1000 randomly selected GZ2 volunteers after fiducial SWAP assessment. Circle size is proportional to the number of gold standard subjects each volunteer classified. The histograms on top and right represent the distribution of each component of the confusion matrix for all volunteers. A quarter of GZ2 volunteers are “Astute”; they correctly identify both ‘Featured’ and ‘Not’ subjects more than 50% of the time. The peaks at 0.5 in both distributions are due primarily to volunteers who see only one training image: only half of their confusion matrix is updated.

2.2.2 Fiducial SWAP simulation

Before we run a simulation, a number of SWAP parameters must be chosen: the initial confusion matrix for each volunteer’s agent, $(P(“F”|F), P(“N”|N))$; the subject prior probability, p_0 ; and the retirement thresholds, t_F and t_N . For our fiducial simulation, we initialize all confusion matrices at $(0.5, 0.5)$, and set the subject prior probability, $p_0 = 0.5$. We set the ‘Featured’ threshold, t_F , i.e., the minimum probability for a subject to be retired as ‘Featured’, to 0.99. Similarly, we set the ‘Not’ threshold, $t_N = 0.004$. In Appendix ?? we show that varying these parameters has only a small affect on the SWAP output. To simulate a live project, we run SWAP on a time step of $\Delta t = 1$ day, during which SWAP processes all volunteer classifications with timestamps within that range. This is performed for three months worth of GZ2 classification data.

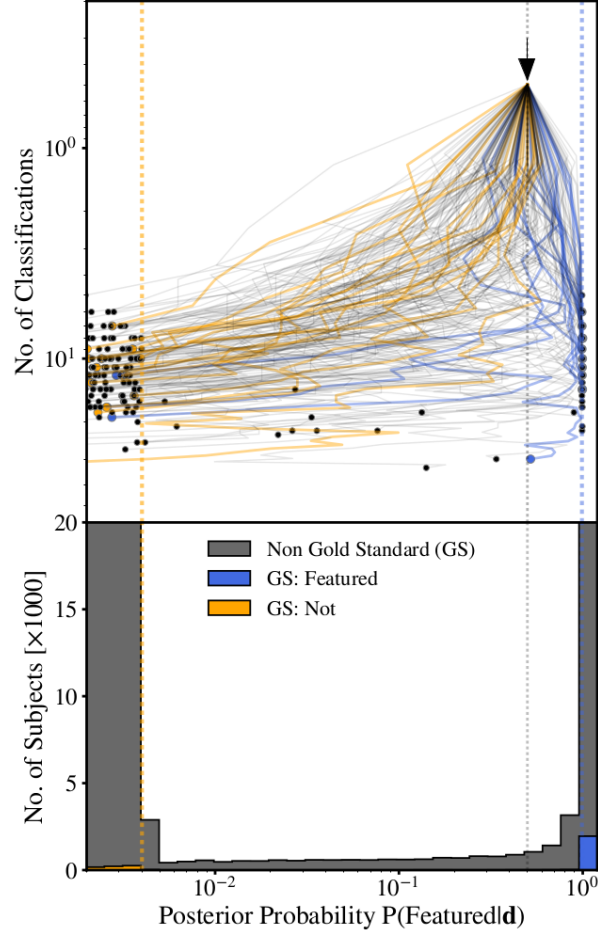


Figure 2.2 Posterior probabilities for GZ2 subjects. The top panel depicts the probability trajectories of 200 randomly selected GZ2 subjects. All subjects begin with a prior of 0.5 denoted by the arrow. Each subject's probability is nudged back and forth with each volunteer classification. From left to right the dotted vertical lines show the 'Not' threshold, prior probability, and 'Featured' threshold. Different colours denote different types of subjects. The bottom panel shows the distribution in probability for all GZ2 subjects by the end of our simulation, where the y axis is truncated to show detail.

Figure 2.1 (adapted from Figure 4 of Marshall et al. 2016) demonstrates the volunteer assessment we achieve, and shows confusion matrices for 1000 randomly selected volunteers. The circle size is proportional to the number of gold standard subjects each

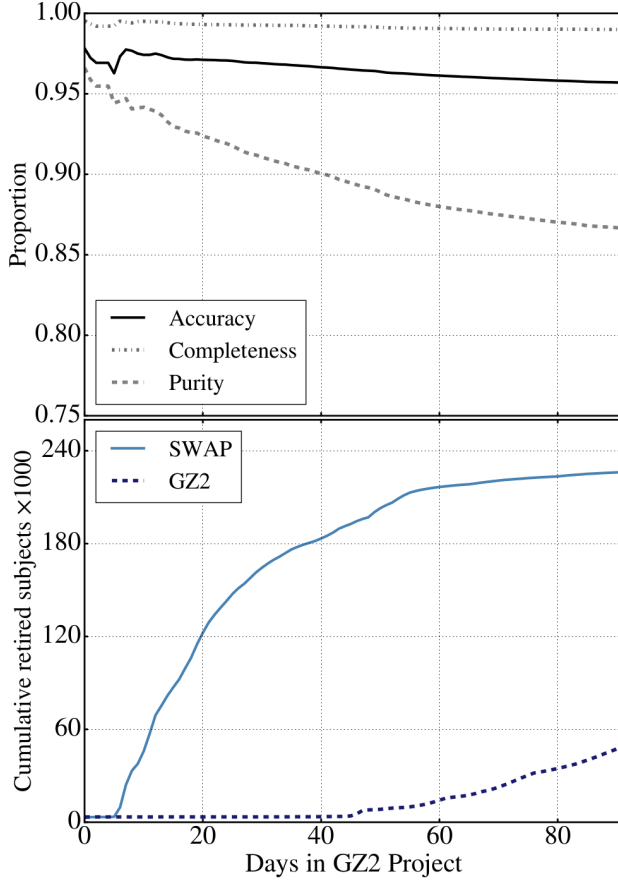


Figure 2.3 Fiducial SWAP simulation demonstrates a factor of 4-5 increase in the rate of subject retirement as a function of GZ2 project time (bottom panel, light blue) compared with the original GZ2 project (dashed dark blue). After 92 days, SWAP retires over 225K subjects, while GZ2 retires ~ 48 K. The top panel displays the quality metrics (greys). These are calculated by comparing SWAP-assigned labels to $GZ2_{\text{raw}}$ labels (Section 2.1) for the subject sample retired by that day of the simulation. Thus, on the final day, SWAP retires 226,124 subjects with 95.7% accuracy, and with completeness and purity of ‘Featured’ subjects at 99% and 86.7% respectively. The decrease in purity as a function of time is due, in part, to the fact that more difficult to classify subjects are retired later in the simulation.

volunteer classified. The histograms represent the distribution of each component of the confusion matrix for all volunteers. Nearly 25% of volunteers are considered “Astute” indicating they correctly identify both ‘Featured’ and ‘Not’ subjects more than 50% of

the time. Furthermore, as long as a volunteer’s confusion matrix is different from random, they provide useful information to the project. The spikes at 0.5 in the histograms are due to volunteers who see only one gold standard subject (i.e., ‘Featured’), leaving their probability in the other (‘Not’) unchanged. Additionally, 4% of volunteers have a confusion matrix of (0.5, 0.5) indicating these volunteers classified two gold standard subjects of the same type, one correctly and one incorrectly.

Figure 2.2 (adapted from Figure 5 of Marshall et al. 2016) demonstrates how subject posterior probabilities are updated with each classification. The arrow in the top panel denotes the prior probability, $p_0 = 0.5$. With each classification, that prior is updated into a posterior probability creating a trajectory through probability space for each subject. The blue and orange lines show the trajectories of a random sample of ‘Featured’ and ‘Not’ subjects from our gold standard sample, while the black lines show the trajectories of a random sample of GZ2 subjects that were not part of the gold standard sample. The similarly coloured vertical dashed lines correspond to the retirement thresholds, t_F and t_N . The lower panel shows the full distribution of GZ2 subject posteriors at the end of our simulation, where the y-axis has been truncated to show detail. An overwhelming majority of subjects cross one of these retirement thresholds.

Our goal is to increase the efficiency of galaxy classification. We therefore use as a metric the cumulative number of retired subjects as a function of the original GZ2 project time. We define a subject as GZ2-retired once it achieves at least 30 volunteer votes, encompassing 98.6% of GZ2 subjects. In contrast, a subject is considered SWAP-retired once its posterior probability crosses either of the retirement thresholds defined above.

However, it is important not to prioritize efficiency at the expense of quality. We thus also consider the metrics of accuracy, purity and completeness as a function of GZ2 project time. These are defined as follows: accuracy is the number of correctly identified subjects divided by the total number retired; completeness is the number of correctly identified ‘Featured’ subjects divided by the number of actual ‘Featured’ retired; and purity is the number of correctly identified ‘Featured’ subjects divided by the number of subjects retired as ‘Featured’. Thus, a complete sample has no false negatives whereas a pure sample has no false positives. We compute these metrics by comparing the SWAP-assigned labels of the cumulatively retired subject set to the GZ2_{raw} labels for

each day of the simulation. For example, by Day 20, SWAP retires 120K subjects with 96% accuracy, 99.7% completeness, and 92% purity.

Figure 2.3 and Table 4.1 detail the results of our fiducial SWAP simulation compared to the original GZ2 project. The bottom panel shows the cumulative number of retired subjects as a function of GZ2 project time. By the end of our simulation, GZ2 (dashed dark blue) retires ~ 50 K subjects while SWAP (solid light blue) retires 226,124 subjects. We thus classify 80% of the entire GZ2 sample in three months. Here we consider the number of classifications logged each day and not the length of time spent on a single classification. Under the assumption that collapsing the GZ2 decision tree to a single question would not have decreased the number of classifications collected each day during the GZ2 project, processing volunteer classifications through SWAP presents a striking increase in classification efficiency. The top panel of Figure 2.3 demonstrates the quality of those classifications as a function of time and establishes that our full SWAP-retired sample is 95.7% accurate, 99% complete, and 86.7% pure. We discuss these small discrepancies in Section 2.2.4.

2.2.3 Reducing human effort

The SWAP algorithm effectively weights volunteers according to how many gold standard subjects they correctly identify. This mechanism provides a reduction in the amount of human effort required to perform this classification task. To see this, we consider a toy model wherein we simulate volunteers with fixed confusion matrices. We simulate 1000 ‘Featured’ subjects and 1000 ‘Not’ subjects each with prior, $p_0 = 0.5$. We simulate 100 volunteer agents all with the same fixed confusion matrix of (0.63, 0.65), where these values are computed as the average $P(“F”|F)$ and $P(“N”|N)$ from our assessment of real volunteers, excluding the spikes at 0.5. We generate volunteer classifications based on this confusion matrix (i.e., volunteers will correctly identify ‘Featured’ subjects 63% of the time) and update the subject’s posterior probability with each classification. We track how many classifications are required for each subject’s posterior to cross either the ‘Featured’ or ‘Not’ retirement thresholds.

The results are presented in Figure 2.4. The filled blue and orange histograms show the number of volunteer classifications per subject achieved from our simulation of GZ2 data, where volunteer agent confusion matrices are those from Figure 2.1. The

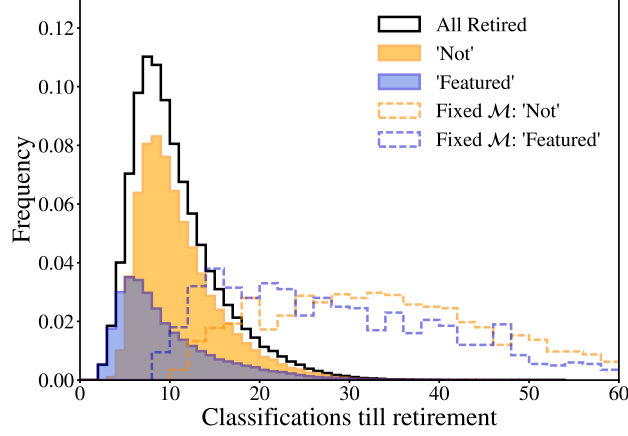


Figure 2.4 SWAP’s volunteer-weighting mechanism provides a factor of three reduction in the human effort required to retire GZ2 subjects. The filled histograms show the number of volunteer classifications per subject achieved from our simulation of GZ2 data broken down by class label, where the solid black line is the total. The dashed histograms are results from our toy model in which we simulate volunteers with fixed confusion matrices, effectively disengaging SWAP’s volunteer-weighting mechanism. These broad distributions require ~ 3 times more classifications per subject to reach the same retirement thresholds.

dashed blue and orange distributions are the results from our toy model. When SWAP accounts for volunteer skill, most subjects are retired with between 6 and 15 votes, with a median of 9 votes. In contrast, when every volunteer is given equal weighting, subjects require 16 to 45 votes with a median of 30 votes before crossing one of the retirement thresholds. Thus the volunteer weighting scheme embedded in SWAP can reduce the amount of human effort required to retire subjects by a factor of three.

This reduction will be, in part, a function of the number of gold standard subjects each volunteer sees. Our gold standard sample was chosen to be representative of morphology rather than evenly distributed among GZ2 volunteers. We thus find that half of our volunteers classify only one or two gold standard subjects. That we achieve a factor of three reduction when only half of our volunteer pool has seen ≥ 2 gold standard subjects suggests that an additional reduction of human effort is possible with more extensive volunteer training.

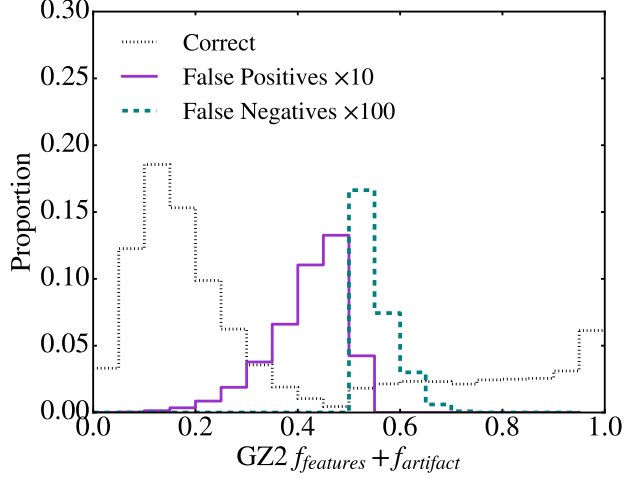


Figure 2.5 Distribution of GZ2 $f_{\text{featured}} + f_{\text{artifact}}$ vote fractions for subjects correctly identified by SWAP (dotted grey), along with those identified as false positives (solid purple), and false negatives (dashed teal). The false positives and false negatives are scaled by factors of 10 and 100 respectively for easier comparison. From Section 2.1, subjects with values > 0.5 are defined as ‘Featured’, however, the teal distribution indicates that SWAP labels them as ‘Not’. This is not a flaw of SWAP: 68.9% of incorrectly identified subjects have $0.4 \leq f_{\text{featured}} + f_{\text{artifact}} \leq 0.6$ suggesting that GZ2_{raw} labels are simply too uncertain. The overlap between the false positives and negatives is due to subjects that are exactly 50-50; by default these are labelled ‘Not’.

2.2.4 Disagreements between SWAP and GZ2

Galaxy Zoo’s strength comes from the consensus of dozens of volunteers voting on each subject. Processing votes with SWAP reduces the number of classifications to reach consensus. Though we typically recover the GZ2_{raw} label, SWAP disagrees about 5% of the time. We thus examine the false positives (subjects SWAP labels as ‘Featured’ but GZ2_{raw} labels as ‘Not’) and false negatives (subjects SWAP labels as ‘Not’ but GZ2_{raw} labels as ‘Featured’). We explore these subjects in redshift, magnitude, physical size, and concentration. We find no correlation with any of these variables, suggesting that, at least for this galaxy sample, the reliability of morphology depends on factors that are not captured by these coarse measurements. This is perhaps unsurprising since GZ2 subjects were selected from the larger GZ1 sample to be the brightest, largest and

nearest galaxies: precisely those subjects most accessible for visual classification.

Instead we consider the stochastic nature of GZ2 vote fractions, which can be estimated as binomial. Let success be a response of “smooth” and failure be any other response. The 68% confidence interval on a subject with $f_{\text{smooth}} = 0.5$ is then $(0.42, 0.57)$ assuming 40 classifications, each with a probability of 0.5. Figure 2.5 shows the distribution of $f_{\text{featured}} + f_{\text{artifact}}$ for the false positives (solid purple), and the false negatives (dashed teal) compared to the subjects where SWAP and GZ2 agree (dotted grey). Recall that if this value is greater than 0.5, the subject is labelled ‘Featured’. The majority of disagreements between SWAP and GZ2 are for subjects that have $0.4 < f_{\text{featured}} + f_{\text{artifact}} < 0.6$. It is thus unsurprising that SWAP and GZ2 disagree most within the approximate confidence interval of our selected GZ2 threshold. We note that the distribution overlap between false positives and false negatives is due to subjects that do not have a majority; these are labelled ‘Not’ by default.

Two other effects contribute to the disagreement between SWAP and GZ2. First, as the number of classifications used to retire a galaxy decreases, the likelihood of misclassification by random chance increases. Second, disagreement arises due to expert-level volunteers whose confusion matrices are close to 1.0. These volunteers are essentially more strongly weighted, allowing that subject’s posterior to cross a retirement threshold in as few as two classifications. In rare cases, despite training, some expert-level volunteers get it wrong compared to the gold-standard labels. These issues can be mitigated by requiring each subject reach a minimum number of classifications in addition to its probability crossing a retirement threshold, thus combining the best qualities of GZ2 and SWAP.

2.2.5 Summary

We demonstrate a factor of four or more increase in classification efficiency while maintaining 95% accuracy, nearly perfect completeness of ‘Featured’ subjects, and with a purity that can be controlled by careful selection of input parameters to be better than 90% (see Appendix ??). Exploring those subjects wherein SWAP and GZ2 disagree, we conclude that the majority of this disagreement stems from the stochastic nature of GZ2_{raw} labels. We now turn our focus towards incorporating a machine classifier utilizing these SWAP-retired subjects as a training sample.

2.3 Stuff from the appendix – fold into the main text

Initial agent confusion matrix. In our fiducial simulation each volunteer was assigned an agent whose confusion matrix was initialized at $(0.5, 0.5)$, which presumes that volunteers are no better than random classifiers. We perform two simulations wherein we initialize agent confusion matrices as $(0.4, 0.4)$, slightly obtuse volunteers; and $(0.6, 0.6)$, slightly astute volunteers, with everything else remaining constant. Results of these simulations compared to the fiducial run are shown in the left panel of Figure 2.6. We find that SWAP is largely insensitive to the initial confusion matrix both in terms of the subject retirement rate and classification quality.

We retire $\sim 225\text{K} \pm 3.5\%$ subjects as shown by the light blue shaded region in the bottom left panel of Figure 2.6, where the dashed blue line denotes the fiducial run. Predictably, when the confusion matrix probabilities are low, we retire fewer subjects than when these probabilities are high for a given period of time. This is easy to understand since it takes longer for volunteers to become astute classifiers when they are initially given values denoting them as obtuse. Regardless, most volunteers become astute classifiers by the end of the simulation. The top left panel demonstrates our usual quality metrics as computed in Section 2.2.2. The dashed lines again denote the fiducial run. We maintain $\sim 95\%$ accuracy, 99% completeness, and $\sim 84\%$ purity; and no metric changes by $> 2\%$ regardless of initial confusion matrix values.

This spread is due to three effects: 1) subjects can receive an alternate SWAP label in different simulations, 2) subjects can be retired in a different order, and 3) the set of retired subjects is not guaranteed to be common to all runs. We find SWAP to be highly consistent: more than 99% of retired subjects are the same among all simulations, and, of these, 99% receive the same label. Instead we find that the order in which subjects are retired changes between runs. When the confusion matrix is low, subjects take longer to classify compared to the fiducial run (i.e., they retire on a later date in GZ2 project time). Likewise, subjects retire sooner when the confusion matrix is high. This can cause quality metrics to vary since they are calculated on a day to day basis. These effects each contribute less than one per cent variation and thus we see a high level of consistency between simulations.

Of interest, perhaps, is that the quality metrics for these simulations are not symmetric about the fiducial run. However, in the Bayesian framework of SWAP, an agent with confusion matrix (0.4, 0.4) contributes as much information as an agent with confusion matrix (0.6, 0.6). The quality metrics computed are thus within a per cent of each other. In either case, we find that initializing agents at (0.5, 0.5) provides optimal performance for the ‘training’ we simulate with our current approach. Further assessment would require a live project with real-time training and feedback.

Subject prior probability, p_0 . The prior probability assigned to each subject is an educated guess of the frequency of that characteristic in the scope of the data at hand. For galaxy morphologies, this number should be an estimate of the probability of observing a desired feature (bar, disk, ring, etc.). In our case, we desire simply to find galaxies that are ‘Featured’; however, this is dependent on mass, redshift, physical size, etc. The original GZ2 sample was selected primarily on magnitude and redshift. As there was no cut on galaxy size (with the exception that each galaxy be larger than the SDSS PSF), the sample includes a large range of masses and sizes. Designating a single prior is not clear-cut; we thus explore how various p_0 values effect the SWAP outcome.

We run simulations allowing p_0 to take values 0.2, 0.35, and 0.8 and compare these to the fiducial run, with everything else remaining constant. The results are shown in the right panels of Figure 2.6. We again find that SWAP is consistent in terms of subject retirement which varies by only 1%. However, as can be seen in the top panel, the variation in our quality metrics is more pronounced. Firstly, though we retire nearly the same number of subjects over the course of each simulation, they are less consistent than our previous runs. That is, only 95% of retired subjects are common to all simulations. Secondly, of those that are common, only 94% receive the same label from SWAP indicating that changing the prior is more likely to produce a different label for a given subject than changing the initial agent confusion matrix. Finally, there is also a larger spread for the day on which a subject is retired as compared to the fiducial run. These trends all contribute to a broader spread in accuracy, completeness, and purity as a function of project time. We stress, however, that although more substantial than the previous comparison, these variations are all within $\pm 5\%$.

We can understand these variations more intuitively by considering the following. Recall that our retirement thresholds, t_F and t_N , have not changed in these simulations.

When p_0 is small, the subject’s probability is already closer to t_N in probability space, and thus more subjects are classified as ‘Not’ compared to the fiducial run. Similarly, when p_0 is large, some of these same subjects can instead be classified as ‘Featured’ because p_0 is already closer to t_F . Obviously, both outcomes cannot be correct. We find that the simulation with $p_0 = 0.8$ performs the worst of any run; this is a direct reflection of the fact that this prior is not suitable for this question or this dataset. Indeed, the best performance is achieved when $p_0 = 0.35$. This reflects the distribution of ‘Featured’ subjects as determined by GZ2_{raw} labels and is more characteristic of the expected proportion of ‘Featured’ galaxies in the local universe. As a value far from the correct value can have a significant impact on the classification quality, it is important to choose a prior wisely.

Retirement thresholds, t_F and t_N . Retirement thresholds are directly related to the time that a subject will spend in SWAP before retirement. If we lower t_F (and/or raise t_N), more subjects will be retired compared to the fiducial run as each subject will have a smaller swath of probability space in which to fluctuate before crossing one of these thresholds. On the other hand, if we raise t_F (and/or lower t_N), it will take longer for subjects to cross one of these thresholds. This also increases the likelihood of some subjects never crossing either threshold, instead oscillating indefinitely through probability space.

What thresholds should one choose? To answer this question, we consider the left panel of Figure 4.7, which depicts the receiver operating characteristic (ROC) curve for our fiducial simulation, an illustration of performance as a function of a threshold for a binary classifier. ROC curves display the true positive rate against the false positive rate for a discriminatory threshold or score with a perfect classifier achieving 100% true positives and no false positives. The value of the threshold optimal for predicting class labels would be that which allows the ROC curve to reach the upper-left-most point in the diagram. We have two thresholds to consider and thus we plot the curve twice: once under the assumption that “true positives” denote correctly identified ‘Featured’ subjects; and again under the assumption that “true positives” instead denote correctly identified ‘Not’ subjects. In both cases, the colour of the line corresponds to the subject posterior probability. We mark the location of $t_F = 0.99$ and $t_N = 0.004$ from our fiducial run with a red triangle and blue square respectively. We see that t_F is nearly

optimal but t_N could be improved upon.

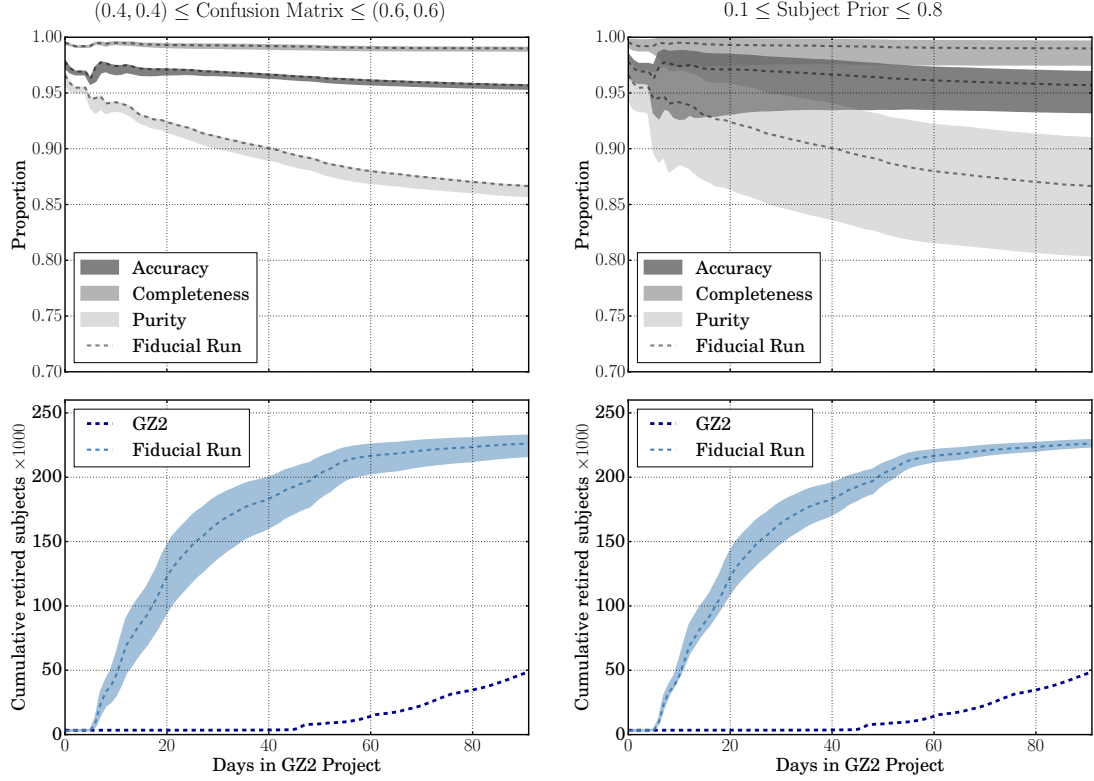


Figure 2.6 SWAP performance does not dramatically change even with a range of input parameters (shaded regions) as compared to the fiducial run of Section 2.2.2 (dashed lines). *Left.* The quality (top) and retirement rate (bottom) when the confusion matrix is initialized as $(0.4, 0.4)$ and $(0.6, 0.6)$, with all other input parameters remaining constant. *Right.* Same as the left panel but allowing the subject prior probability, $p_0 = 0.2, 0.35$ and 0.8 . Changing the confusion matrix has little impact on the quality of the labels but varies the total number of subjects retired. In contrast, changing the subject prior is more likely to affect the classification quality rather than the total number of subjects retired.

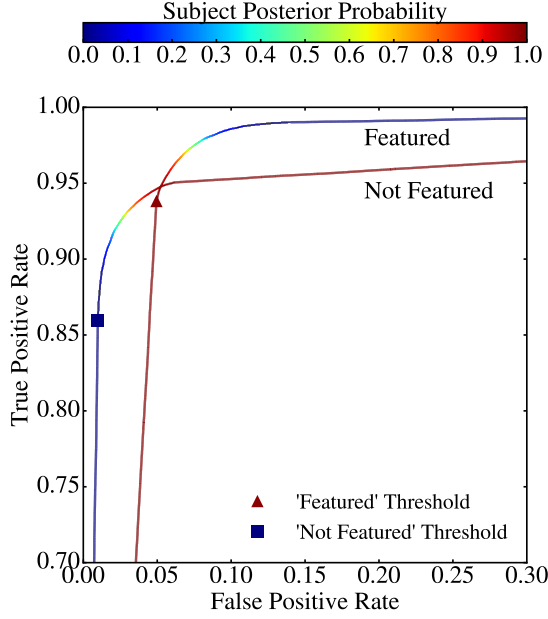


Figure 2.7 *Left*. Identifying ‘Featured’ subjects is independent of identifying ‘Not’ subjects. Both ROC curves use all subjects processed by SWAP where the score used to create the ROC curve is simply each subject’s achieved posterior probability. The Featured curve demonstrates how well we identify ‘Featured’ subjects with a threshold of 0.99, while the Not Featured curve demonstrates how well we identify ‘Not’ subjects with a threshold of 0.004. Typically, best performance is achieved by the score associated with the upper-left-most part of the curve. Our ‘Featured’ threshold is nearly optimal, while our ‘Not’ threshold could be improved since the blue square is not as close to the upper left hand corner as other possible values of the subject posterior. *Right*. Relation between measured morphology diagnostics for more than 280K SDSS galaxies. Most of these galaxies are processed through SWAP, receiving a posterior probability that estimates how likely each is to be ‘Featured’ or ‘Not’.

Chapter 3

Measuring Nonparametric Morphological Diagnostics on SDSS Stamps

3.1 Introduction

Any machine classifier must have a set of features from which to learn to differentiate between classes. These features can be anything: pixel values, spectra, anything that can correlate well enough with the class boundary that the machine can learn that boundary. Choosing which features are most appropriate for each task is not necessarily straight-forward or easy. Too few features, and the machine will not be able to learn the things that define each class. Too many features and machine training time could increase substantially or, worse, training will be subjected to the Curse of Dimensionality: with increasing parameter space dimensionality, the number of samples required to learn that parameter space increases exponentially!

In this work we draw on the Zurich Estimator of Structural Types (ZEST (Scarlata et al., 2007)). ZEST utilized five features measured from the light profile of galaxy imaging combined with a PCA analysis to determine morphology for 120K COSMOS galaxies. These features are well known to correlate strongly with the distinction between early- and late-type galaxies. In this chapter we discuss how we measure these

same features for the SDSS galaxy sample of GZ2.

3.2 Data

We obtain *i*-band imaging from SDSS Data Release 12 for all XXX galaxies in the GZ2 project. [WHY *i*-band?].

Along with imaging, we also obtain basic SDSS measurements for each galaxy including the Petrosian radius. This value is used to create postage stamps from the SDSS fields for each galaxy with dimensions of 3 Petrosian radii. Galaxies located within 3 Petrosian radii of the edge of a field were excluded as we did not perform mosaicing. This removed only XXX galaxies from our sample.

3.3 Image Cleaning

Postage stamps undergo a cleaning process whereby nearby sources are identified with SExtractor (ver. 2.8.6; Bertin & Arnouts, 1996) and their pixels replaced with values that mimic the background in that region.

3.4 Morphology Diagnostics

We compute the following widely adopted nonparametric measurements of the galaxy light distribution on the cleaned postage stamps:

Concentration is computed as $C = 5 \log(r_{80}/r_{20})$ where r_{80} and r_{20} are the radii containing 80% and 20% of the galaxy light respectively. Small values of this ratio tend to indicate disk galaxies, while larger values correlate with early-type ellipticals.

Asymmetry quantifies the degree of rotational symmetry in the galaxy light distribution (not necessarily the physical shape of the galaxy as this parameter is not highly sensitive to low surface brightness features). A correction for background noise is applied (as in e.g. Conselice et al. (2000)), i.e.,

$$A = \frac{\sum_{x,y} |I - I_{180}|}{2 \sum |I|} - B_{180} \quad (3.1)$$

where I is the galaxy flux in each pixel (x, y) , I_{180} is the image rotated by 180 degrees about the galaxy's central pixel, and B_{180} is the average asymmetry of the background.

The Gini coefficient, G , (Glasser, 1962; Abraham et al., 2003) describes how uniformly distributed a galaxy’s flux is. If G is 0, the flux is distributed homogeneously among all galaxy pixels; if G is 1, the light is contained within a single pixel. This term correlates with C , however, G does not require that the flux be in the central region of the galaxy. We follow Lotz et al. (2004) by first ordering the pixels by increasing flux value, and then computing

$$G = \frac{1}{|\bar{X}|n(n-1)} \sum_i^n (2i - n - 1) |X_i| \quad (3.2)$$

where n is the number of pixels assigned to the galaxy, and \bar{X} is the mean pixel value.

M_{20} (Lotz et al., 2004) is the second order moment of the brightest 20% of the galaxy flux. We compute it as

$$M_{tot} = \sum_i^n f_i [(x_i - x_c)^2 + (y_i - y_c)^2] \quad (3.3)$$

$$M_{20} = \log_{10}\left(\frac{\sum_i M_i}{M_{tot}}\right), \quad \text{while } \sum_i f_i < 0.2 f_{tot} \quad (3.4)$$

where M_{tot} , the total moment, is computed first and f_{tot} is the total flux. For centrally concentrated objects, M_{20} correlates with C but is also sensitive to bright off-centre knots of light.

Finally, we use the ellipticity, $\epsilon = 1 - b/a$, of the light distribution as measured by SExtractor which computes the semi-major axis a and semi-minor axis b from the second-order moments of the galaxy light.

In total, we measure morphological indicators for 282,350 SDSS galaxies. The relations between these diagnostics for the full sample is shown in the right panel of Figure 4.7. The code developed to clean and compute these morphology indicators is open source and can be found at https://github.com/melaniebeck/measure_morphology.

3.5 Comparison with other samples

Chapter 4

Combining nonparametric morphologies with human and machine intelligence

4.1 Efficiency through incorporation of machine classifiers

We construct the full Galaxy Zoo Express by incorporating supervised learning, the machine learning task of inference from labelled training data. The training data consist of a set of training examples, and must include an input feature vector and a desired output label. Generally speaking, a supervised learning algorithm analyses the training data and produces a function that can be mapped to new examples. A properly optimized algorithm will correctly determine class labels for unseen data. By processing human classifications through SWAP, we obtain a set of binary labels by which we can train a machine classifier. We briefly outline the technical details of our machine below, turning towards the decision engine we develop in Section 4.1.4.

4.1.1 Random Forests

We use a Random Forest (RF) algorithm (Breiman, 2001), an ensemble classifier that operates by bootstrapping the training data and constructing a multitude of individual decision tree algorithms, one for each subsample. An individual decision tree works

by deciding which of the input features best separates the classes. It does this by performing splits on the values of the input feature that minimize the classification error. These feature splits proceed recursively. Decision trees alone are prone to over-fitting, precluding them from generalizing well to new data. Random Forests mitigate this effect by combining the output labels from a multitude of decision trees. Specifically, we use the `RandomForestClassifier` from the Python module `scikit-learn` (Pedregosa et al., 2011).

4.1.2 Grid Search and Cross-validation

Of fundamental importance is the task of choosing an algorithm’s hyperparameters, values which determine how the machine learns. For a RF, key quantities include the maximum depth of individual trees (`max_depth`), the number of trees in the forest (`n_estimators`), and the number of features to consider when looking for the best split (`max_features`). The goal is to determine which values will optimize the machine’s performance and thus these values cannot be chosen *a priori*. We perform a grid search with k -fold cross-validation whereby the training sample is split into k subsamples. One subsample is withheld to estimate the machine’s performance while the remaining data are used to train the machine. This is performed k times and the average performance value is recorded. The entire process is repeated for every combination of the hyperparameters in the grid space and values that optimize the output are chosen. In this work we let $k = 10$, however, we leave this as an adjustable input parameter. In the interest of computational speed, we set `n_estimators` = 30 and perform the grid search for `max_depth` over the range $[5, 16]$, and `max_features` over the range $[\sqrt{D}, D]$, where D is the number of features in the feature vector, described below.

4.1.3 Feature Representation and Pre-Processing

The feature vector on which the machine learns is composed of D individual numeric quantities associated with the subject that the machine uses to discern that subject from others in the training sample. To segregate ‘Featured’ from ‘Not’, we draw on ZEST (Scarlata et al., 2007) and compute concentration, asymmetry, Gini coefficient, and M_{20} , the second-order moment of light for the brightest 20% of galaxy pixels as

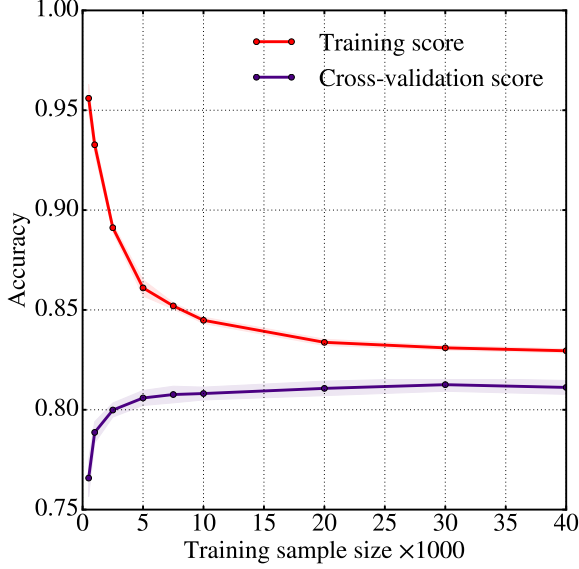


Figure 4.1 Learning curve for a Random Forest with fixed hyperparameters. These curves show the mean accuracy computed during cross-validation and on the training sample, where the shaded regions denote the standard deviation. When the training sample size is small, the machine accurately identifies its own training sample but is unable to generalize to unseen data as evidenced by a low cross-validation score. As the training sample size increases, the cross-validation score increases. This behaviour plateaus indicating that larger training samples provide little in additional performance.

measured from SDSS DR12 *i*-band imaging (see Appendix ??). Coupled with SExtractor’s measurement of ellipticity (Bertin & Arnouts, 1996), we provide the machine with a $D = 5$ dimensional morphology parameter space. These non-parametric diagnostics have long been used to distinguish between early- and late-type galaxies in an automated fashion (e.g., Abraham et al., 1996; Bershadsky et al., 2000; Conselice et al., 2000; Abraham et al., 2003; Conselice, 2003; Lotz et al., 2004; Snyder et al., 2015). Because the RF algorithm handles a variety of input formats, the only pre-processing step we perform is the removal of poorly-measured morphological indicators, i.e. catastrophic failures.

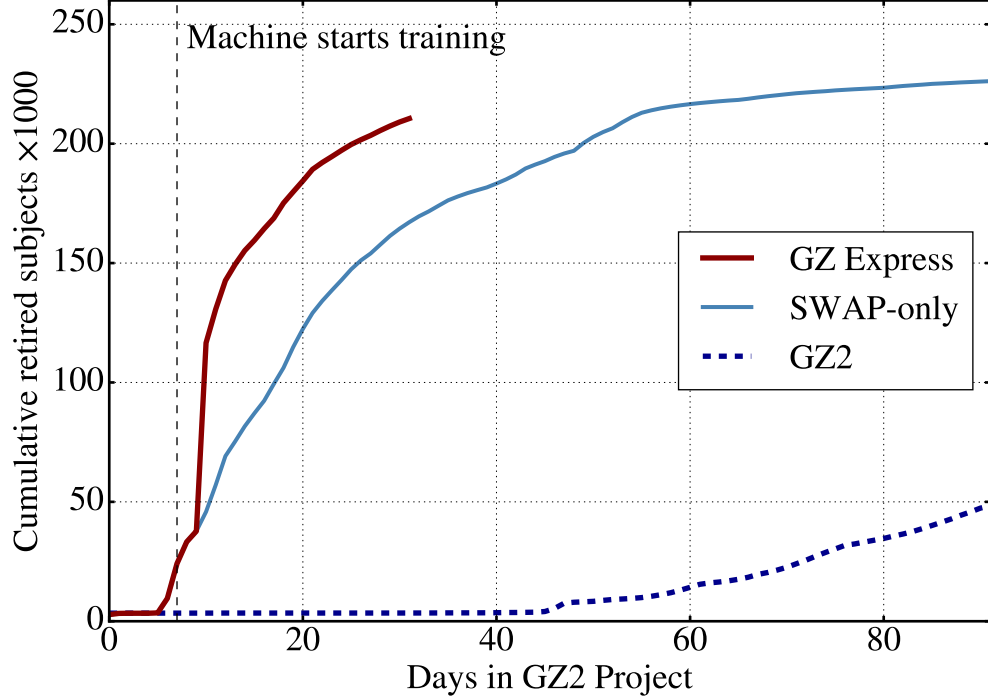


Figure 4.2 By incorporating a machine classifier, GZX (red) increases the classification rate by an order of magnitude compared to GZ2 (dashed dark blue) and out-performs the SWAP-only run (light blue), retiring more than 200K subjects in just 27 days of GZ2 project time. The dashed black line marks the first night the machine trains. After several additional nights of training, it is deemed optimized and allowed to retire subjects. Both humans and machine then contribute to retirement. We end the simulation after 32 days having retired over 210K galaxies. See Table 4.1 for details.

4.1.4 Decision Engine

A number of decisions must be addressed before attempting to train the machine. In particular, which subjects should be designated as the training sample? When should the machine attempt its first training session? When has the machine’s performance been optimized such that it will successfully generalize to unseen subjects? The field of machine learning provides few hard rules for answering these questions, only guidelines and best practices. Here we briefly discuss our approach for the development of our decision engine.

As discussed in detail in Section 2.2, SWAP yields a probability that a subject exhibits the feature of interest. While some machine algorithms can accept continuous input labels, the RF requires distinct classes. We thus use only those subjects which have crossed either of the retirement thresholds. Though we find that SWAP consistently retires 35-40% ‘Featured’ subjects on any given day of the simulation, a balanced ratio of ‘Featured’ to ‘Not’ isn’t guaranteed. Highly unbalanced training samples should be resampled to correct the imbalance; however, as we exhibit only a mild lopsidedness, we allow the machine to train on all SWAP-retired subjects.

SWAP retires a few hundred subjects during the first days of the simulation. In principle, a machine can be trained with such a small sample, but will be unable to generalize to unseen data. We estimate a minimum number of training samples and the machine’s ability to generalize by considering a learning curve, an illustration of a machine’s performance with increasing sample size for fixed hyperparameters. Figure 4.1 demonstrates such a curve wherein we plot the accuracy from both the 10-fold cross-validation, and the trained machine applied to its own training sample for a random sample of GZ2 subjects required to be balanced between ‘Featured’ and ‘Not’. We fix the RF’s hyperparameters as follows: `max_depth` = 8, `n_estimators` = 30, and `max_features` = 2. When the sample size is small, the cross-validation score is low and the training score is high, a clear sign of over-fitting. However, as the training sample size increases, the cross-validation score increases and eventually plateaus, indicating that larger training sets will yield little additional gain.

We estimate this plateau begins when the training sample reaches 10,000 subjects and require SWAP retire at least this many before the machine attempts its first training. We estimate the machine has trained sufficiently if the cross-validation score fluctuates by less than 1% for three consecutive nights of training to ensure we have reached the plateau. This requires that we record the machine’s training performance each night, including how well it scores on the training sample, the cross-validation score, and the best hyperparameters.

4.1.5 The Machine Shop

We can now describe a full GZX simulation, which begins with human classifications processed through SWAP for several days. Once at least 10K subjects have been retired,

their feature vectors are passed to the machine for its inaugural training. A suite of performance metrics are recorded by a machine agent, similar in construction to SWAP’s agents. This agent determines when the machine has trained sufficiently by assessing the variation in performance metrics for all previous nights of training. Once the machine has been optimized, the agent introduces it to the test sample consisting of any subject that has not yet reached retirement through SWAP and is not part of the gold standard sample.

Analogous to SWAP, we generate a retirement rule for machine-classified subjects. In addition to the class prediction, the RF algorithm computes the probability for each subject to belong to each class. This probability is simply the average of the probabilities of each individual decision tree, where the probability of a single tree is determined as the fraction of subjects of class X on a leaf node. Only subjects that receive a class prediction of ‘Featured’ with $p_{\text{machine}} \geq 0.9$ ($p_{\text{machine}} \leq 0.1$ for ‘Not’) are considered retired. The remaining subjects have the possibility of being classified by humans or the machine on a future night of the simulation. This constitutes the core of our passive feedback mechanism. Subjects that are not retired by the machine can instead be retired by humans, thus providing the machine a more fully sampled morphology parameter space on future training sessions.

4.2 Results

We perform a full GZX simulation incorporating our RF with the fiducial SWAP run discussed in Section 2.2.2. The machine attempts its first training on Day 8 with an initial training sample of $\sim 20\text{K}$ subjects. It undergoes several additional nights of training, each time with a larger training sample. By Day 12, SWAP has provided over 40K subjects for training and the machine’s agent has deemed the machine optimized. The machine predicts class labels for the remaining 230K GZ2 subjects. Of those, the machine retires over 70K, dramatically increasing the subset of retired subjects. We end the simulation after 32 days, having retired $\sim 210\text{K}$ subjects as detailed in Table 4.1.

We present these results in Figure 4.2 where subject retirement with GZX (red) is compared to our fiducial SWAP-only run (light blue) and GZ2 (dashed dark blue). Using the GZ2_{raw} labels as before, we compute our usual quality metrics on the full

sample of GZX-retired subjects; reported in Table 4.1. Accuracy and purity remain within a few percent of the SWAP-only run at 93.5% and 84.2% respectively. Instead we see a 5% decline in the completeness. While the SWAP-only run identified 99% of ‘Featured’ subjects, incorporation of the machine seems to miss a significant portion thus dropping GZX completeness to 94.3%. We discuss this behaviour below.

By dynamically generating a training sample through a more sophisticated analysis of human classifications coupled with a machine classifier, we retire more than 200K GZ2 subjects in just 27 days. Visual classification through SWAP alone retires as many in 50 days, while GZ2 requires a full year. Though our analysis considers only the top-level task of GZ2’s decision tree, GZX suggests a tantalizing potential to increase the classification rate by an order of magnitude over the traditional crowd-sourced approach. We next explore the composition of those classifications.

4.2.1 Who retires what, when?

In the top panel of Figure 4.3 we explore the individual contributions to GZX subject retirement from the RF (dash-dotted teal) and SWAP (dashed orange). The solid black line shows the total GZX retirement (SWAP+RF), while the dotted grey line depicts the fiducial SWAP-only run from Section 2.2.2 for reference. Two things are immediately obvious. First, each component shoulders approximately half of the retirement burden with the machine and SWAP responsible for $\sim 100\text{K}$ and $\sim 110\text{K}$ subjects respectively. Secondly, the rate of retirement exhibited by the two components is in stark contrast. SWAP retires at a relatively constant rate while the machine retires dramatically at the beginning of its application, quickly surpassing the human contribution, and plateaus thereafter. We thus clearly see three epochs of subject retirement. In the first phase, humans are the only contributors to subject retirement. Once the machine is optimized, it immediately contributes more to retirement than humans. However, the machine’s performance plateaus quickly; the third phase is again dominated by human classifications.

In the bottom panels of Figure 4.3, we consider the class composition of subjects retired by SWAP and the RF. The left (right) panel shows the retired fraction of GZ2 subjects identified as ‘Featured’ (‘Not’) according to their GZ2_{raw} labels as a function of GZ2 project time. Overall, GZX retires 73.6% of the GZ2 subject sample and this is

Table 4.1 Summary of key quantities for GZ2 and our various simulations. All quality metrics are calculated using GZ2_{raw} labels.

Simulation Summary						
	Days	Subjects Retired	Human Effort (classifications)	Accuracy (%)	Purity (%)	Completeness (%)
Galaxy Zoo 2	430	285962	16,340,298	–	–	–
SWAP only	92	226124	2,298,772	95.7	86.7	99.0
SWAP+RF	32	210543	932,017	93.5	84.2	94.3

evenly distributed between ‘Featured’ and ‘Not’ subjects as indicated by the solid black lines in both panels. However, SWAP retires more than 50% of all ‘Featured’ subjects while the machine retires only 18%. This divergence does not exist for ‘Not’ subjects where each component contributes 33-37%.

What is the source of this discrepancy? Each night the machine trains on a sample composed consistently of 30-40% ‘Featured’ subjects but does not retire a similar proportion, indicating that the 30% of non-retired ‘Featured’ subjects do not receive high p_{machine} . In the following section we explore whether this is an artefact of our choice in machine or in the human-machine combination implemented here.

4.2.2 Machine performance

Throughout our analysis we have defined ‘Featured’ and ‘Not’ subjects by their GZ2_{raw} labels as this was the most compatible choice for comparison with SWAP output. However, the machine does not learn in the same way, nor is it presented with the same information. Machine and human classifications each provide valuable and complementary information for identifying ‘Featured’ galaxies.

We isolate the 6127 subjects that were deemed false positives, i.e., galaxies retired by the machine as ‘Featured’ that have ‘Not’ GZ2_{raw} labels, a sample that comprises only 6.25% of all subjects the machine retires. We visually examine several hundred and assess that, to the expert eye, a majority are, in fact, ‘Featured’. A random sample is shown in Figure 4.4.

That the machine strongly identifies these galaxies as ‘Featured’ ($p_{\text{machine}} \geq 0.9$) where humans instead classify them as ‘Not’ ($f_{\text{featured}} < 0.5$) has several contributing

factors: 1) as discussed in Section 2.2.4, the threshold we chose carries with it a confidence interval such that subjects with $0.4 < f_{\text{featured}} + f_{\text{artifact}} < 0.6$ are most likely to receive disagreeing labels from other classifying agents, 2) the first task of the GZ2 decision tree asks a question that does not necessarily correlate with a split between early- and late-type galaxies, and 3) the machine learns on morphology diagnostics that are very different from visual inspection.

We find that 41.4% of these false positives have $0.4 \leq f_{\text{featured}} + f_{\text{artifact}} < 0.5$ indicating that the disagreement between humans and machine is likely due to the labels we assign at our given threshold. However, we also find that 43.5% of false positives have $f_{\text{featured}} + f_{\text{artifact}} \leq 0.35$, and this discrepancy is not as easily explained. In Figure 4.4 we examine a random sample of false positives in this regime where, for clarity, we display only the f_{featured} value in the lower left corner. The majority of these subjects are discs lacking features such as spiral arms or strong bars. Whether this is the reason the majority of volunteers classify these objects as “smooth” is beyond the scope of this paper, however, this behaviour might be modified by providing actual training images and live feedback as performed in Marshall et al. (2016). We suggest that, at least for this particular question, if either human or machine identifies a subject as ‘Featured’, it is likely the subject is discy and worth further investigation.

Accordingly, this suggests that, in some cases, the morphology indicators we measure are sufficient for the machine to recognize ‘Featured’ galaxies regardless of the labels humans provide. Figure 4.5 shows the distribution of each morphology indicator for all subjects the machine retires as ‘Featured’ (blue) and ‘Not’ (orange) compared to the full GZ2 subject set. The difference between ‘Featured’ and ‘Not’ is stark in all but the M_{20} distribution. This can be seen explicitly in Figure 4.6 in which we show the RF’s ranked feature importances, where large values indicate higher importance. Feature importance is computed as how much each feature decreases the impurity of a split in a tree. The impurity decrease from each feature is then averaged over all trees and ranked. We show the feature importance averaged over all nights of training with black bars indicating the standard deviation. The machine finds the Gini coefficient most important for class prediction, placing little emphasis on M_{20} . It is well known that the Gini coefficient is more sensitive to noise than other diagnostics, however, we point out that when a machine is faced with two or more correlated features any of them

can be used as the predictor. Once chosen, the importance of the others is reduced. This explains why Concentration is ranked much lower than Gini even though they are strongly correlated as seen in Figure 4.7. That the machine relies heavily on these two morphology diagnostics is unsurprising as concentration has long been an automated predictor between early- and late-type galaxies (Abraham et al., 1994, 1996; Shen et al., 2003).

The complementary nature of human and machine classification can best be utilized by a feedback mechanism in which a portion of machine-retired subjects are reviewed by humans. Subjects that display excessive disagreement should be verified by an expert (or expert-user). In the same way that humans increase the machine’s training sample over time, subjects that the machine properly identifies can become part of the humans’ training sample.

4.3 Looking Forward

We have demonstrated the first practical framework for combining human and machine intelligence in galaxy morphology classification tasks. While we focus below on a brief discussion of our next steps and potential applications to large upcoming surveys, we note that our results have implications for the future of citizen science and Galaxy Zoo in particular.

GZX is perhaps one of the simplest ways to combine human and machine intelligence and its impressive performance motivates a higher level of sophistication. A first step will be an implementation of SWAP that can handle a complex decision tree. In addition, we envision multiple forms of active feedback in addition to our passive feedback mechanism. SWAP allows us to leverage the most skilled volunteers to review galaxies difficult for either human or machine to classify. Additionally, machine-retired subjects should contribute to the training sample for humans in an analogous fashion to what we have already implemented.

Secondly, our RF can be improved by providing it information equal to what humans receive: multi-band morphology diagnostics will be included in our future feature vector. However, the Random Forest algorithm is not easily adapted to handle measurement errors or class labels with continuous distributions. To fully utilize the information

provided by SWAP, sophisticated algorithms should be considered such as deep convolutional neural networks (CNN) or Latent Dirichlet allocation (LDA), an algorithm that is frequently used in document processing. Furthermore, there is no reason to limit to a single machine. As hinted at in Figure 1.1, several machines could train simultaneously, their predictions aggregated through SWAP, creating an on-the-fly machine ensemble.

With the above upgrades implemented, we expect performance of both the classification rate and quality to further increase. However, even our current implementation can cope with upcoming data volumes from large surveys. By some estimates, *Euclid* is expected to obtain measurable morphology with its visual instrument (VIS) for approximately $10^6 - 10^7$ galaxies (Laureijs et al., 2011). Visual classification at the rate achieved with Galaxy Zoo today would require 12–120 years to classify.¹ If the *Euclid* sample is on the high end, GZX as currently implemented could classify the brightest 20% during the six years of its observing mission. As currently implemented, we obtain accuracy around 95% potentially leaving hundreds of thousands of galaxies with unreliable classifications. In a companion paper that seeks to identify supernovae, Wright et al. (submitted) demonstrate a dramatic increase in accuracy through an entirely different human-machine combination whereby the scores from human and machine are averaged together with the combined score yielding the most reliable classification. Again, a combination of both approaches will allow us to take full advantage of legacy output from large scale surveys.

4.3.1 Conclusions

In this paper we design and test Galaxy Zoo Express, an innovative system² for the efficient classification of galaxy morphology tasks that integrates the native ability of the human mind to identify the abstract and novel with machine learning algorithms that provide speed and brute force. We demonstrate for the first time that the SWAP algorithm, originally developed to identify rare gravitational lenses in the Space Warps project, is robust for use in galaxy morphology classification. We show that by implementing SWAP on GZ2 classification data we can increase the rate of classification by a factor of 4-5, requiring only 90 days of GZ2 project time to classify nearly 80% of the

¹ We note that the classification rate of GZ2 was 4 times higher than GZ’s current steady rate.

² Our code can be found at <https://github.com/melaniebeck/GZExpress>

entire galaxy sample.

Furthermore, we have implemented and tested a Random Forest algorithm and developed a decision engine that delegates tasks between human and machine. We show that even this simple machine is capable of providing significant gains in the classification rate when combined with human classifiers: GZX retires over 70% of GZ2 galaxies in just 32 days of GZ2 project time. This represents a factor of 11.4 increase in the classification rate as well as an order of magnitude reduction in human effort compared to the original GZ2 project. This is achieved without sacrificing the quality of classifications as we maintain accuracy well above 90% throughout our simulations. Additionally, we have shown that training on a 5-dimensional parameter space of traditional non-parametric morphology indicators allows the machine to identify subjects that humans miss, providing a complementary approach to visual classification. The gain in classification speed allows us to tackle the massive amount of data promised from large surveys like *LSST* and *Euclid*.

4.4 Acknowledgements

MB thanks Steven Bamford and Boris Häußler for insightful discussions on citizen science and Galaxy Zoo; and John Wallin and Marc Huertas-Company for several enlightening conversations on machine learning and classification. We are grateful to Elisabeth Baeten, Micaela Bagley, Karlen Shahinyan, Vihang Mehta, Steven Bamford, Kevin Schawinski, and Rebecca Smethurst for providing expert classifications in addition to those provided by the authors. PJM acknowledges Aprajita Verma and Anupreeta More for their ongoing collaboration on the Space Warps project.

MB, CS, LF, KW, and MG gratefully acknowledge support from the US National Science Foundation Grant AST-1413610. MB acknowledges additional support through New College and Oxford University’s Balzan Fellowship as well as the University of Minnesota Doctoral Dissertation Fellowship. Travel funding was supplied to MB, in part, by the University of Minnesota Thesis Research Travel Grant. CJL recognizes support from a grant from the Science & Technology Facilities Council (ST/N003179/1). BDS acknowledges support from Balliol College, Oxford, and the National Aeronautics and

Space Administration (NASA) through Einstein Postdoctoral Fellowship Award Number PF5-160143 issued by the Chandra X-ray Observatory Center, which is operated by the Smithsonian Astrophysical Observatory for and on behalf of NASA under contract NAS8-03060. The work of PJM is supported by the U.S. Department of Energy under contract number DE-AC02-76SF00515.

4.5 Stuff to fold into the existing text

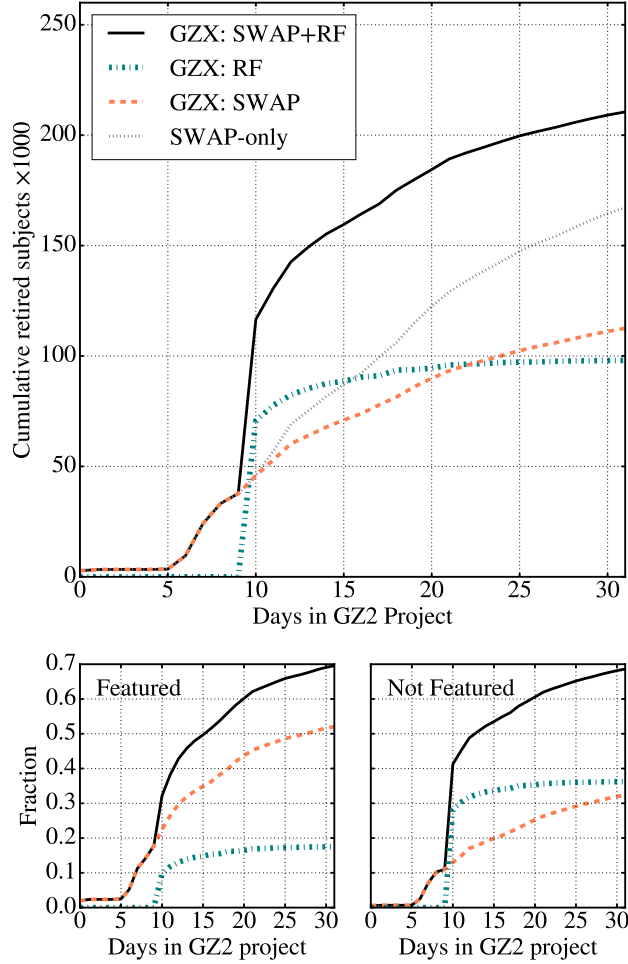


Figure 4.3 Contributions to subject retirement by both classifying agents of GZX: human (SWAP) and machine. The top panel shows cumulative subject retirement for GZX as a whole (solid black), along with that attributed to the RF (dash-dotted teal), and SWAP (dashed orange). The dotted grey line shows the fiducial SWAP-only run for comparison. Retirement totals for humans and machine are nearly equal over the course of the simulation but display different behaviours: SWAP’s retirement rate is almost constant while the RF contributes substantially after its initial application and then plateaus. The bottom panels show what fraction of GZ2 subjects are retired, separated by class label. Overall, GZX retires 73.6% of the entire GZ2 sample in 32 days, retiring the same proportion of ‘Featured’ and ‘Not’ subjects as indicated by the black lines. However, humans retire 30% more ‘Featured’ subjects than the machine, while both components retire a similar proportion of ‘Not’ subjects.

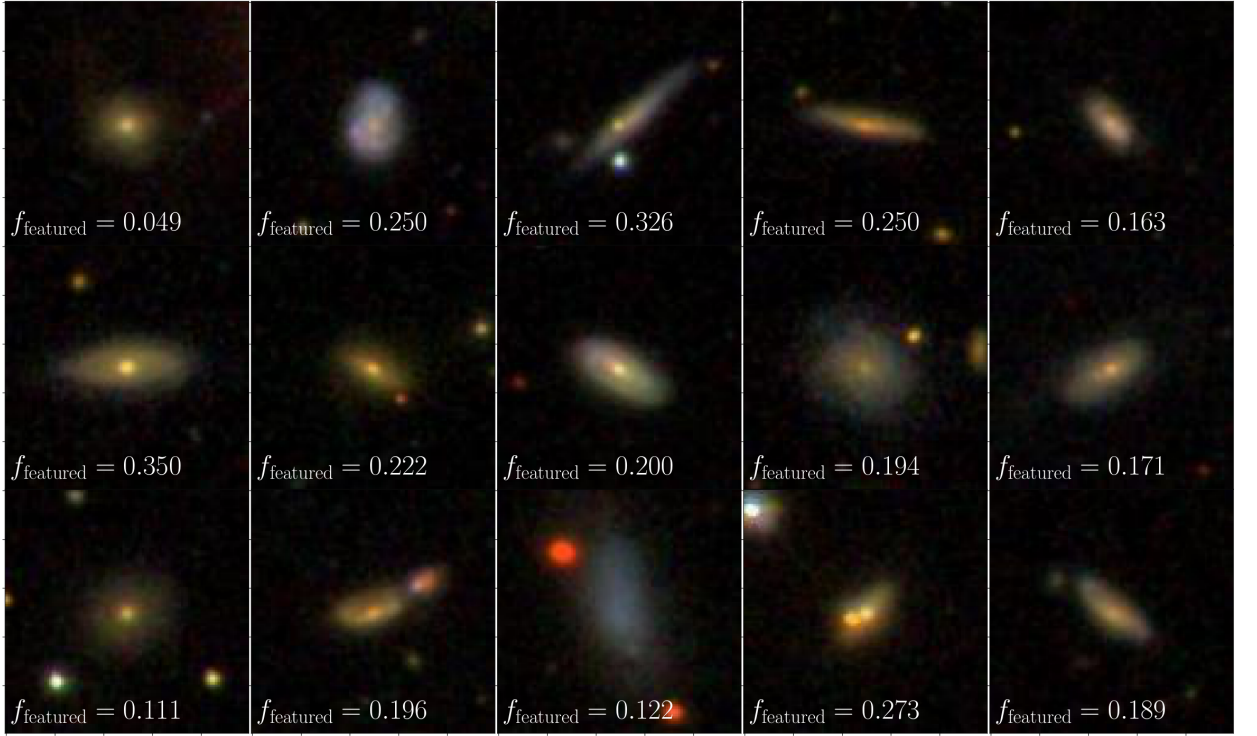


Figure 4.4 A random subsample of subjects identified as false positives: labelled by machine as ‘Featured’, but as ‘Not’ according to $GZ2_{\text{raw}}$. We display f_{smooth} in the lower left corner, that is, the fraction of volunteers who classified the subject as ‘smooth’ (‘Not’). Values are typically between 0.5 and 0.65 indicating that GZ2 volunteers did not reach a strong consensus. Fortunately, the machine is able to identify these subjects as ‘Featured’ due to their measured morphology diagnostics.

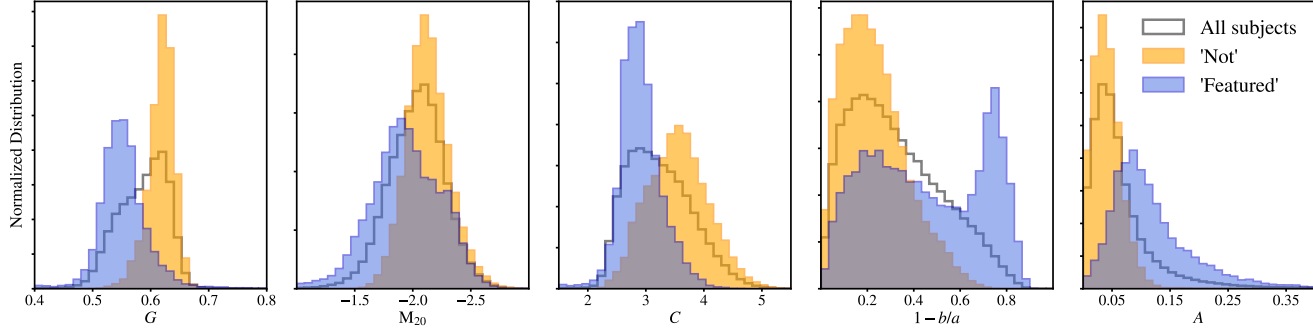


Figure 4.5 The RF is trained on a 5-dimensional morphology parameter space. We show the distribution of each morphology indicator for machine-retired ‘Featured’ (blue) and ‘Not’ (orange) subjects compared to the full GZ2 subject sample (black). The difference between ‘Featured’ and ‘Not’ subjects is in stark contrast for all distributions except, perhaps, M_{20} .

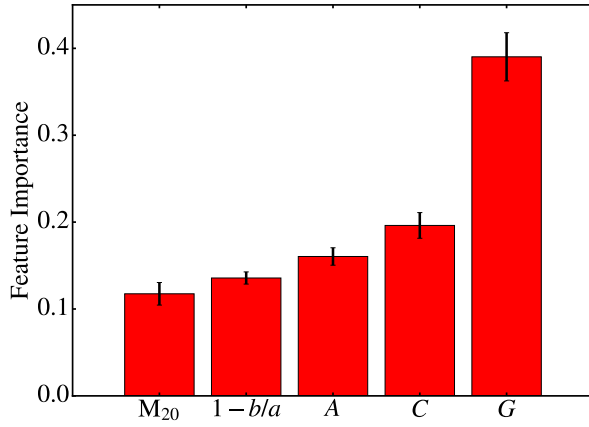


Figure 4.6 The RF’s ranked feature importance averaged over all nights of training with black bars indicating the standard deviation. A larger value corresponds to higher importance. The machine computes feature importance according to how much each feature increases the purity of the resulting split averaged over all trees in the forest. The RF places great importance in the Gini coefficient though we note that it can under-represent the importance of highly correlated features such as concentration.

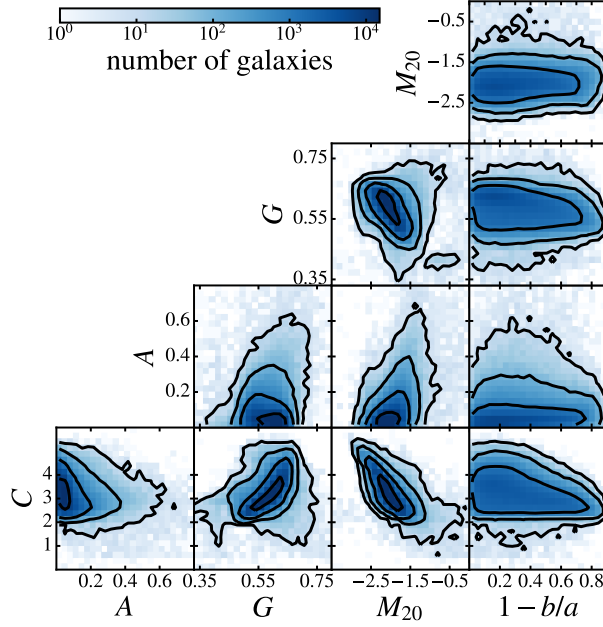


Figure 4.7 *Left*. Identifying ‘Featured’ subjects is independent of identifying ‘Not’ subjects. Both ROC curves use all subjects processed by SWAP where the score used to create the ROC curve is simply each subject’s achieved posterior probability. The Featured curve demonstrates how well we identify ‘Featured’ subjects with a threshold of 0.99, while the Not Featured curve demonstrates how well we identify ‘Not’ subjects with a threshold of 0.004. Typically, best performance is achieved by the score associated with the upper-left-most part of the curve. Our ‘Featured’ threshold is nearly optimal, while our ‘Not’ threshold could be improved since the blue square is not as close to the upper left hand corner as other possible values of the subject posterior. *Right*. Relation between measured morphology diagnostics for more than 280K SDSS galaxies. Most of these galaxies are processed through SWAP, receiving a posterior probability that estimates how likely each is to be ‘Featured’ or ‘Not’.

Chapter 5

A population of “clumpy” galaxies in local Universe

All the things about clumps.

5.1 Sample Selection & Data

What was put into Galaxy Zoo: Hubble? All of Stripe 82 (but what does that mean?)
Why were they put in?

From Willett+17:

Single-epoch images from SDSS Stripe 82 were selected using the criteria from Willett et al. 2013, which required limits of `petroR90_r` $> 3''$ and a magnitude brighter than $m_r < 17.77$. 21,522 galaxies in SDSS met these criteria. Co-added images from Stripe 82 were selected from the union of galaxies with co-added magnitudes brighter than 17.77 mag, and the galaxies detected in the stripe-82-single images and matched to a co-add source. This resulted in a total set of 30,339 images. Of the images in the co-added sample, 5144 (17%) were dimmer than the initial cut of 17.77 mag.

Delicious side-effect: Clumpies!

We consider the Stripe 82 subjects that were part of the GZH project. The GZH catalog doesn’t provide debiased labels for the Stripe 82 subjects, most likely because this has already been done before in GZ2 and because the debiasing is completely different for these low redshift subjects. If we’re now going to pick out subjects that are

“featured” – shouldn’t we use the debiased GZ2 values? How much does this change our sample? For that matter, how similar are the smooth and featured vote fractions between GZ2 and GZH? **Not going to answer this question in this paper.**

To select a sample of “clumpy” galaxies from the GZH Stripe 82 sample, we consider only those subjects with high featured and high clumpy vote fractions; the fraction of volunteers who classified each subject as being featured or clumpy. Specifically, we began with a selection criteria of $f_{\text{featured}} \geq 0.5$ and $f_{\text{clumpy}} \geq 0.5$ and $N_{\text{votes}} \geq 20$, where N_{votes} is the number of volunteers who answered the question “Does the galaxy have a mostly clumpy appearance?”. This produced a sample of 629 galaxies: 273 with single-epoch imaging and 356 with coadd imaging. After visual inspection we find that this is hardly a pure sample of traditional clumpy galaxies instead including many small groups of elliptical galaxies as well as galaxies in various merging states and possessing multiple nuclei. [show example image?] After excluding these and duplicate imaging, we retain 90 coadd-depth clumpy galaxies and 102 single-depth clumpy galaxies. Of these, 36 subjects have both single- and coadd-depth imaging.

[Note: technically ALL of these galaxies have single- and coadd-depth imaging because they are all in Stripe82. it’s only a point of contention here because not all of them have the GZH morphologies assigned to them, for various reasons.]

We next select only those subjects which have spectroscopic redshift $z < 0.06$. Beyond this distance, the physical scale as observed with SDSS imaging is no longer similar to Hubble’s at $z \sim 3$. The physical scale at $z = 0.06$ is $1'' = 1.1 \text{ kpc}$. SDSS pixel scale is $0.396''/\text{pixel}$. $\approx 0.43 \text{ kpc/pixel} \approx 2.3 \text{ pixels} = 1 \text{ kpc}$. Our final sample contains 105 unique galaxies, each with at least one SDSS spectrum. Half of our sample consist of objects with multiple spectra. We visually inspect these to verify that the SDSS fiber was indeed positioned over a star-forming region rather than the galactic bulge or other structure.

We obtain SDSS DR12 *ugriz* coadd imaging and spectra within $30''$ for every galaxy in our sample, discarding those spectra which belong to nearby sources or stars. We find that one “clumpy” galaxy is, in fact, a juxtaposition of three galaxies at disparate redshifts flagged as clumpy due to the low resolution of SDSS imaging. We exclude this subject(s) from our sample. Our final list includes 175 spectra. Approximately half of the galaxies in our sample have more than one SDSS spectrum with a handful having

three or four spectra.

5.2 Analysis

During visual inspection we discover that several of the galaxies in our sample have very low surface brightness. Additionally, extremely bright clumps and nearby sources make SDSS photometry (and, subsequently, stellar masses) suspect. In this section we describe our analysis of basic galaxy parameters.

We create postage stamps of each galaxy from each field and all bands of our SDSS coadd imaging. The cutout sizes are determined to be 5 times the petrosian radius as computed by the SDSS pipeline. As mentioned above, however, this pipeline fails to properly account for galaxy extent and thus produces unrealistic measurements of the petrosian radius. We visually inspect all of our cutouts and choose an appropriate postage stamp size that fully encompasses each galaxy. The postage stamp radius is determined from the r-band petrosian radius and this value is used as the stamp size for each band.

We next process the r-band (maybe g-band cuz that's more blue?) postage stamp with Source Extractor (Bertin and whoever) using parameters designed to detect low surface brightness features. Important parameters are detailed in Table X that doesn't exist yet. Though these parameters adequately identify most of our sample, galaxies that fail are redone individually and SE parameters are tweaked for each particular case. These segmentation maps define the galaxy extent for all future analysis.

5.2.1 Measuring clump radial distance

5.2.2 Clump H α H β ratios [Dust]

5.2.3 Clumpy H α equivalent widths

5.3 Discussion / Conclusions

our clumps are the best clumps. Everybody says so.

We thank all the people who contributed to Galaxy Zoo.

Chapter 6

Summary & Future Work

The goal of this thesis was to study the mass-loss histories of hypergiants stars using new capabilities in near-IR imaging and polarimetry, and airborne mid-IR imaging. With LBT/LMIRCam and MMT-Pol on the MMT we have imaged the nebulae of VY CMa and IRC +10420 with sub-arcsecond resolution, revealing recent mass-loss in the close environments around these stars. To probe further into these hypergiants' past history, we have used mid-infrared imaging with SOFIA/FORCAST to search for cold dust and performed 1-D radiative transfer modeling of their SEDs and resolved profiles.

Our $2 - 5 \mu\text{m}$ adaptive optics imaging of the cool hypergiant VY CMa penetrates deeper into its dusty nebula than in the optical, probing its recent mass-loss history. In Chapter 2 we analyzed the resolved images of its peculiar “Southwest” Clump, which has no obvious counterpart on the opposite side of the star. The distinct shape of the SW Clump is suggestive of a short-lived, localized event and may be analogous to a coronal mass ejection (CME) from a single location on the Sun’s surface. A short-lived ejection event is consistent with the SW Clump appearing as a confined, coherent shape several hundred years after ejection. Using adaptive optics imaging polarimetry, in Chapter 3 we demonstrated the Clump is optically thick through at least $3.1 \mu\text{m}$ and reaffirmed the lower limit mass of $5 \times 10^{-3} M_{\odot}$ based on modeling its surface brightness as optically thick scattered light. Our $1.3 \mu\text{m}$ polarimetry detects several other prominent features of VY CMa’s nebula include the NW Arc, Arc 2, S Knot, and S Arc. Using the polarized intensity as a lower limit on total scattered light intensity, we found each of these features to be optically thick as well. Their relatively high intrinsic polarizations

are consistent with their high scattering optical depths since the depolarizing effect of multiple scatters is reduced for typical silicate grain albedos. In Chapter 4, we used 20 – 37 μm infrared imaging with SOFIA/FORCAST to search for evidence of earlier mass loss. VY CMa’s morphology at the longest wavelengths coincides with the general shape of the highly asymmetric nebulae seen in the visual, suggesting thermal emission from dust associated with the expanding arcs to the northwest and southwest. Modeling its SED we computed an average mass-loss rate of $6 \times 10^{-4} M_{\odot} \text{ yr}^{-1}$ over the past ~ 1200 years, with no clear evidence of mass loss much farther in its past.

Our study of the warm hypergiant IRC +10420 similarly traced its mass-loss over a range of angular scales. At the sub-arcsecond scale using adaptive optics, in Chapter 3 we used 2.2 μm polarimetry to reveal a relatively uniform nebula largely in the plane of the sky extending out to $2''.5$ from the star. This low-latitude ejecta is optically thick. Combining the polarimetry with 3 – 5 μm imaging that shows extended emission, we modeled the flux of this nebula and found its emission is an order of magnitude brighter than can be explained by simple extrapolation of the scattered light seen at 2.2 μm . We hypothesized grains warmed to a temperature higher than the expected grain equilibrium temperature, but consistent with the local gas temperature in this region. In Chapter 4 we presented 8 – 12 μm adaptive optics images that reveal spatially extended emission spanning nearly the same range as the 2.2 μm polarimetry. Applying radiative transfer modeling to the intensity profile of this extended emission and the SED, we found that IRC +10420’s mass-loss history is divided into two distinct periods. Our best-fit model showed that it lost mass at a high average rate of $2 \times 10^{-3} M_{\odot} \text{ yr}^{-1}$ from 6000 – 2000 yr ago during its presumed RSG stage, followed by an order of magnitude decrease to an average rate of $1 \times 10^{-4} M_{\odot} \text{ yr}^{-1}$ in the past 2000 yr.

In addition to VY CMa and IRC +10420, our SOFIA/FORCAST program included the RSG μ Cep and the warm hypergiant ρ Cas. Our study of μ Cep probes a mass-loss history extending back $\sim 13,000$ yr. To match the observed intensity profile of its resolved nebula in FORCAST 25 – 37 μm images, our radiative transfer modeling requires a declining mass-loss rate. We find that over the 13,000 yr dynamical age of the shell, its mass loss-rate has declined from 5×10^{-6} to $1 \times 10^{-6} M_{\odot} \text{ yr}^{-1}$. In contrast to the high mass-loss rate of VY CMa, μ Cep’s rate is significantly lower than RSGs of comparable luminosity. In the case of ρ Cas, we demonstrated that our new 19.7 –

37.1 μm SOFIA/FORCAST photometry are consistent with the continued expansion and thinning of the dust shell formed as a result of the 1946 eruption. We did not find evidence of new dust formation from more recent eruptions.

In the future, infrared imaging over a range of angular scales will be used to expand the sample of RSGs and post-RSGs with resolved mass-loss. The SOFIA/FORCAST Cycle 3 program 03_0082 (PI: R. Humphreys) included three additional RSG targets (NML Cyg, VX Sgr and S Per) and contingent approval has been granted for observations of the yellow hypergiant HR 5171A during a Cycle 4 Southern deployment if flight scheduling permits. In Fall 2016, VY CMa is scheduled for observation with NOMIC, the 8 – 13 μm imager on the Large Binocular Telescope. With NOMIC’s 0''.27 angular resolution (for single dish observing mode), VY CMa’s SW Clump should be resolved. These observations will better sample the Clump’s SED and could help resolve the puzzle of its non-detection by ALMA reported in ?.

The work presented in this thesis has demonstrated the capabilities of MMT-Pol and LMIRCam to resolve circumstellar ejecta around RSGs and post-RSGs. These capabilities will be extended to several recently identified RSG clusters, each of which contains substantial coeval RSG populations. These include RSGC1 (??), RSGC2 = Stephenson 2 (?), NGC 7419 (?) and the Per OB1 association, which contains many RSGs in its halo including S Per (?). Imaging these clusters of RSGs in polarized intensity in the near-infrared with MMT-Pol will cleanly separate light scattered by dusty nebulae from the stars’ light, and when combined with adaptive optics imaging from 3 – 13 μm with LMIRCam/NOMIC will enable us to trace the RSGs mass-loss. Since the RSG cluster populations are coeval, this will allow the role of high mass loss events on their evolution to be studied.

References

- Abraham, R. G., Tanvir, N. R., Santiago, B. X., et al. 1996, MNRAS, 279, L47
- Abraham, R. G., Valdes, F., Yee, H. K. C., & van den Bergh, S. 1994, ApJ, 432, 75
- Abraham, R. G., van den Bergh, S., & Nair, P. 2003, ApJ, 588, 218
- Baillard, A., Bertin, E., de Lapparent, V., et al. 2011, A&A, 532, A74
- Ball, N. M., Loveday, J., Fukugita, M., et al. 2004, MNRAS, 348, 1038
- Bamford, S. P., Nichol, R. C., Baldry, I. K., et al. 2009, MNRAS, 393, 1324
- Banerji, M., Lahav, O., Lintott, C. J., et al. 2010, MNRAS, 406, 342
- Bershady, M. A., Jangren, A., & Conselice, C. J. 2000, AJ, 119, 2645
- Bertin, E., & Arnouts, S. 1996, A&AS, 117, 393
- Blanton, M. R., Hogg, D. W., Bahcall, N. A., et al. 2003, ApJ, 594, 186
- Breiman, L. 2001, Machine Learning, 45, 5
- Cardamone, C., Schawinski, K., Sarzi, M., et al. 2009, MNRAS, 399, 1191
- Casteels, K. R. V., Conselice, C. J., Bamford, S. P., et al. 2014, MNRAS, 445, 1157
- Conselice, C. J. 2003, ApJS, 147, 1
- . 2006, MNRAS, 373, 1389
- Conselice, C. J., Bershady, M. A., & Jangren, A. 2000, ApJ, 529, 886

- Darg, D. W., Kaviraj, S., Lintott, C. J., et al. 2010, MNRAS, 401, 1552
- de Vaucouleurs, G. 1959, Handbuch der Physik, 53, 275
- Dieleman, S., Willett, K. W., & Dambre, J. 2015, MNRAS, 450, 1441
- Dressler, A. 1980, ApJ, 236, 351
- Elmegreen, B. G., Bournaud, F., & Elmegreen, D. M. 2008, ApJ, 688, 67
- Elmegreen, B. G., Elmegreen, D. M., Sánchez Almeida, J., et al. 2013, ApJ, 774, 86
- Freeman, P. E., Izbicki, R., Lee, A. B., et al. 2013, MNRAS, 434, 282
- Galloway, M. A., Willett, K. W., Fortson, L. F., et al. 2015, MNRAS, 448, 3442
- Glasser, G. J. 1962, Journal of the American Statistical Association, 57, 648
- Griffith, R. L., Cooper, M. C., Newman, J. A., et al. 2012, ApJS, 200, 9
- Holwerda, B. W., Muñoz-Mateos, J.-C., Comerón, S., et al. 2014, ApJ, 781, 12
- Hubble, E. P. 1936, The Realm of the Nebulae (Yale University Press)
- Huertas-Company, M., Rouan, D., Tasca, L., Soucail, G., & Le Fèvre, O. 2008, A&A, 478, 971
- Huertas-Company, M., Gravet, R., Cabrera-Vives, G., et al. 2015, ApJS, 221, 8
- Kartalpe, J. S., Mozena, M., Kocevski, D., et al. 2015, ApJS, 221, 11
- Kauffmann, G., Heckman, T. M., White, S. D. M., et al. 2003, MNRAS, 341, 54
- Kormendy, J. 1977, ApJ, 217, 406
- Kormendy, J., & Kennicutt, Jr., R. C. 2004, ARA&A, 42, 603
- Land, K., Slosar, A., Lintott, C., et al. 2008, MNRAS, 388, 1686
- Laureijs, R., Amiaux, J., Arduini, S., et al. 2011, ArXiv e-prints, arXiv:1110.3193
- Lintott, C., Schawinski, K., Bamford, S., et al. 2011, MNRAS, 410, 166

- Lintott, C. J., Schawinski, K., Slosar, A., et al. 2008, MNRAS, 389, 1179
- Lotz, J. M., Primack, J., & Madau, P. 2004, AJ, 128, 163
- LSST Science Collaboration, Abell, P. A., Allison, J., et al. 2009, ArXiv e-prints, arXiv:0912.0201
- Marshall, P. J., Verma, A., More, A., et al. 2016, MNRAS, 455, 1171
- Masters, K. L., Nichol, R. C., Hoyle, B., et al. 2011, MNRAS, 411, 2026
- Meert, A., Vikram, V., & Bernardi, M. 2016, MNRAS, 455, 2440
- More, A., Verma, A., Marshall, P. J., et al. 2016, MNRAS, 455, 1191
- Nair, P. B., & Abraham, R. G. 2010, ApJS, 186, 427
- Nakamura, O., Fukugita, M., Yasuda, N., et al. 2003, AJ, 125, 1682
- Odewahn, S. C., Cohen, S. H., Windhorst, R. A., & Philip, N. S. 2002, ApJ, 568, 539
- Pedregosa, F., Varoquaux, G., Gramfort, A., et al. 2011, Journal of Machine Learning Research, 12, 2825
- Peng, C. Y., Ho, L. C., Impey, C. D., & Rix, H.-W. 2002, AJ, 124, 266
- Peng, Y.-j., Lilly, S. J., Kovač, K., et al. 2010, ApJ, 721, 193
- Peth, M. A., Lotz, J. M., Freeman, P. E., et al. 2016, MNRAS, 458, 963
- Sandage, A. 1961, The Hubble atlas of galaxies
- Scarlata, C., Carollo, C. M., Lilly, S., et al. 2007, ApJS, 172, 406
- Schawinski, K., Urry, C. M., Simmons, B. D., et al. 2014, MNRAS, 440, 889
- Sersic, J. L. 1968, Atlas de galaxias australes
- Shen, S., Mo, H. J., White, S. D. M., et al. 2003, MNRAS, 343, 978
- Sheth, K., Elmegreen, D. M., Elmegreen, B. G., et al. 2008, ApJ, 675, 1141

- Simard, L., Mendel, J. T., Patton, D. R., Ellison, S. L., & McConnachie, A. W. 2011, *ApJS*, 196, 11
- Simmons, B. D., Melvin, T., Lintott, C., et al. 2014, *MNRAS*, 445, 3466
- Simmons, B. D., Lintott, C., Willett, K. W., et al. 2017, *MNRAS*, 464, 4420
- Smethurst, R. J., Lintott, C. J., Simmons, B. D., et al. 2016, *MNRAS*, 463, 2986
- Snyder, G. F., Torrey, P., Lotz, J. M., et al. 2015, *MNRAS*, 454, 1886
- Strateva, I., Ivezić, Ž., Knapp, G. R., et al. 2001, *AJ*, 122, 1861
- van den Bergh, S. 1976, *ApJ*, 206, 883
- Watanabe, M., Kodaira, K., & Okamura, S. 1985, *ApJ*, 292, 72
- Whitmore, B. C., Lucas, R. A., McElroy, D. B., et al. 1990, *AJ*, 100, 1489
- Willett, K. W., Lintott, C. J., Bamford, S. P., et al. 2013, *MNRAS*, 435, 2835
- Willett, K. W., Galloway, M. A., Bamford, S. P., et al. 2017, *MNRAS*, 464, 4176

Appendix A

Spectro-polarimetry Confirms Central Powering in a Ly α Nebula at $z = 3.09$

This chapter has been published in The Astrophysical Journal with the following bibliographic reference: Beck, Melanie; Scarlata, Claudia; Hayes, Matthew; Dijkstra, Mark; and Jones, Terry J. 2016, ApJ, 818, 138.